



# Comparing multiple model-derived aerosol optical properties to collocated ground-based and satellite measurements

Ilissa B. Ocko<sup>1</sup> and Paul A. Ginoux<sup>2</sup>

<sup>1</sup>Environmental Defense Fund, New York, 10010, USA

5 <sup>2</sup>NOAA Geophysical Fluid Dynamics Laboratory, Princeton, 08540, USA

*Correspondence to:* Ilissa B. Ocko (iocko@edf.org)

**Abstract.** Anthropogenic aerosols are a key factor governing Earth's climate, and play a central role in human-caused climate change. However, because of aerosols' complex physical, optical, and dynamical properties, aerosols are one of the most uncertain aspects of climate modeling. Fortunately, aerosol measurement networks over the past few decades have led to the establishment of long-term observations for numerous locations worldwide. Further, the availability of datasets from several different measurement techniques (such as ground-based and satellite instruments) can help scientists increasingly improve modeling efforts. This study explores the value of evaluating several model-simulated aerosol properties with data from collocated instruments. We compare optical depth (total, scattering, and absorption), single scattering albedo, Ångström exponent, and extinction vertical profiles in two prominent global climate models to seasonal observations from collocated instruments (AERONET and CALIOP) at seven polluted and biomass burning regions worldwide. We find that models may accurately reproduce one variable while totally failing at another; data from collocated instruments can reveal underlying aerosol-governing physics; column properties may wash out important vertical distinctions; and "improved" models does not mean all aspects are improved. We conclude that it is important to make use of all available data (parameters and instruments) when evaluating aerosol properties derived by models.

## 20 **1 Introduction**

Industrial, residential, transportation, and agricultural activities have considerably increased the amount of aerosols in the atmosphere since the onset of the Industrial Revolution in the mid-19th Century (e.g., Solomon et al., 2007). Atmospheric aerosols are important for Earth's climate because they are comprised of optically scattering and absorbing particles that can also serve as cloud condensation nuclei (e.g., Boucher et al., 2013). Aerosols' capabilities in either reflecting energy out to space through scattering of sunlight, trapping additional energy in the Earth system through absorption of sunlight, reducing insolation at the surface, and modifying cloud properties, can significantly alter Earth's radiation budget and influence climate conditions (e.g., Ocko et al., 2014).

Aerosols have relatively short atmospheric lifetimes – on the order of a week – and therefore their atmospheric distributions are localized near emission sources. The spatial heterogeneities in aerosol distribution lead to strong regional differences in



radiative forcing, and consequentially in regional climate effects (e.g., Ramanathan and Carmichael, 2008; Shindell and Faluvegi, 2009; Bollasina et al., 2011). Further, sources of anthropogenic aerosols are mainly in the Northern Hemisphere, leading to a meridional asymmetry in distributions and aerosol forcings across the two hemispheres. Aerosol's perturbation of the energy balance specifically in the Northern Hemisphere has been shown to influence large-scale circulation as well as  
5 local climate (Bollasina et al., 2011; Ocko et al., 2014).

Aerosol vertical distributions can also influence climate conditions. Radiative forcings are particularly sensitive to vertical distributions of aerosols due to the relative location of clouds, attenuation of insolation, and relative humidity (e.g., Haywood and Ramaswamy, 1998; Samset et al. 2013). The vertical profile of absorbing aerosols, in particular, has a strong bearing on the hydrological cycle (Ming et al., 2010; Ocko et al., 2014).

10 In order to fully understand how aerosols influence climate, it becomes necessary to employ numerical models to simulate aerosol distributions and properties, evaluate their perturbations to the radiative budget, and investigate changes in thermal, hydrological, and dynamical atmospheric and oceanic properties. To build confidence in model results, however, it is important to evaluate aerosol properties against available observations. For the past few decades, long-term time series measurements of global aerosol properties have accumulated from ground-based and satellite instruments. Collocated  
15 instruments provide opportunities to compare model data with multiple datasets, and the retrieval of multiple aerosol properties from some instruments provides opportunities to evaluate several model-derived aerosol parameters.

The Aerosol Comparisons between Observations and Models (AeroCom) project has pioneered aerosol evaluation in numerous chemistry-transport models and global climate models (e.g., Kinne et al., 2006; Koffi et al. 2012), highlighting model diversity of aerosol properties (e.g., Schulz et al. 2006; Koch et al. 2009; Tsigaridis et al. 2014). Earlier AeroCom  
20 studies relied heavily on two-dimensional AEROSOL ROBOTIC NETWORK (AERONET) and Moderate Resolution Imaging Spectroradiometer (MODIS) measurements (Kinne et al. 2006), while recent studies have incorporated three-dimensional Cloud–Aerosol Lidar with Orthogonal Polarization (CALIOP) measurements (eg., Koffi et al. 2012).

Most studies do not take advantage of all available datasets, however a multi-dataset approach can provide a more comprehensive picture (Miller et al., 2011). Here we compare multiple model-simulated aerosol properties from two  
25 prominent climate models to available datasets from collocated ground-based and satellite instruments, in order to evaluate related models with vastly different aerosol treatments. Building off of previous evaluations (Ginoux et al., 2006; Donner et al., 2011; Naik et al., 2013), as well as Ocko et al. (2014) that show the importance of horizontal and vertical distributions of anthropogenic scattering and absorbing aerosols in dominating a suite of climate responses to the forcings, we select seven locations worldwide that represent a diversity of situations in which both anthropogenic sulfate and black carbon are  
30 prevalent. For the purpose of evaluating aerosol optical data simulated by climate models, we seek to determine whether it is



important to compare all parameters with available data and from multiple instruments, or if it is sufficient to select just a few key parameters (e.g., aerosol optical depth) measured by one instrument.

We analyze model properties from two world-renowned climate models from the same development family – NOAA GFDL CM2.1 and CM3. These models have been used for Coupled Model Intercomparison Project (CMIP) 3 and 5 respectively and are included in the Intergovernmental Panel on Climate Change (IPCC) reports. Because the aerosol treatments are starkly different, as we present in section 3, this provides an additional perspective of comparing multiple optical properties with collocated instruments, adding to evaluations performed by Donner et al. (2011) and Naik et al. (2013) that looked at AOD only.

## 2 Observational datasets

We compare present-day model aerosol optical properties (in the visible wavelengths) to observations by ground-based instruments (AERONET) and satellite instruments (CALIOP). We select seven cities worldwide that have long-term seasonal time series of measurements (at least seven years of AERONET data), relatively large amounts of anthropogenic scattering and absorbing aerosols, encompass a range of different anthropogenic conditions (such as slightly polluted vs. majorly polluted), and have global coverage; four of the cities represent industrialized regions, while the other three cities represent biomass burning regions. To represent industrialized areas, we chose data from the Atmospheric Radiation Measurement (ARM) Climate Research Facility in Oklahoma, U.S.; Belsk, Poland; Kanpur, India; and Chen-Kung University in Taiwan. While the ARM facility is located in rural Oklahoma, it is not without influence of upwind pollution as discussed by Andrews et al. (2011). Kanpur, on the other hand, is one of the most polluted cities in the world. Of these four sites, the longest AERONET time-series we use is 16 years in Oklahoma (1994–2010), and the shortest is eight years in Belsk and Taiwan (2002–2010). To represent biomass burning areas, we chose Alta Floresta, Brazil; Mongu, Zambia; and Mukdahan, Thailand. Alta Floresta contains the longest time-series with 19 years (1993–2012), and Mukdahan contains the shortest with seven years (2003–2010). A map of all locations can be found in Fig. 1.

### 2.1 AERONET

The AERosol RObotic NETwork (AERONET) is a ground-based, remote sensing, sun photometer measurement network with more than 300 stations worldwide (Holben et al., 1998, 2001). Originally established by the National Aeronautics and Space Administration (NASA) in the 1990s, it has been greatly expanded by other institutions and offers long-term, continuous, and readily accessible data. AERONET provides direct measurements of aerosol optical depth (AOD) and the Ångström exponent ( $\alpha$ ), and uses inverse algorithms to derive further optical properties such as scattering AOD, absorption AOD, and single-scattering albedo. There are eight wavelength filters. To isolate AOD from other atmospheric gases and particles, the radiation attenuation due to Rayleigh scattering and absorption by ozone and gaseous pollutants is estimated and



removed. Three measurements are taken 30 seconds apart, six to nine times a day. We use the level 2 data, which are quality assured and cloud screened (Smirnov et al., 2000).

We compare AERONET measurements of AOD, scattering AOD, absorption AOD, SSA, and  $\alpha$  to the parameters derived by the CM2.1 and CM3 models for all seven cities, as these locations represent different environments with strong anthropogenic influence. The AERONET AOD in the visible spectrum is measured at 440 nm (blue), whereas the model AOD in the visible spectrum is only archived at 550 nm (green) wavelength. Black carbon and dust will be more impacted by the 440/550 nm difference than sulfate, because of their spectral variation across the visible and near-UV spectrum. For example, black carbon absorbs more in the green than the blue part of the solar spectrum, whereas the opposite is true for dust. However, we do not expect the differences to affect the comparison as the errors are not expected to be large. We use the inverse products derived from the Dubovik algorithm (Dubovik and King, 2000; Dubovik et al., 2002; Dubovik et al., 2006). While AERONET retrievals of AOD are greatly accurate, additional properties derived from inverse algorithms are subject to random noise, systematic errors, instrumental offsets, and uncertainties in the radiation model (Dubovik et al., 2000). Further, we did not interpolate the model data for each AERONET site which would improve comparisons.

## 2.2 CALIOP

The Cloud–Aerosol Lidar with Orthogonal Polarization (CALIOP) is an instrument aboard the Cloud–Aerosol Lidar and Infrared Pathfinder Satellite Observation (CALIPSO) satellite, launched in 2006 (Winker et al., 2007). CALIOP employs LIDAR to measure vertical profile AOD and extinction at two wavelengths (532 nm and 1064 nm). Global monthly gridded level 3 data are available from 2007 to 2011 with a vertical resolution of 30–60 m and a horizontal resolution of 333 m. We use the latest version 3 data that have been described and validated by Winker et al. (2013). AeroCom’s evaluation with CALIOP data used level 2 data from 2007 to 2009 (Koffi et al., 2012). Version 3 provides a more robust comparison than that by Level 2 due to numerous algorithm improvements, significant bugs fixed, and calibration improvements. CALIOP Level-3 2x5 degree grid has a monthly temporal resolution. Errors in CALIOP data are due to a combination of many factors, such as instrument calibration and offsets, cloud contamination, low signal-to-noise ratio, and uncertainties in multiple scattering, LIDAR ratio, molecular number density, and accumulated aerosol attenuation (Winker et al., 2013). We compare monthly extinction vertical profile measurements at 532 nm to the model estimates (at 550 nm) for the industrialized and biomass burning sites.

## 3 Model description and simulations

The National Oceanic and Atmospheric Administration (NOAA) Geophysical Fluid Dynamics Laboratory (GFDL) CM2.1 model (Delworth et al., 2006) and CM3 model (Donner et al., 2011; Griffies et al., 2011) are employed for this analysis. CM2.1 is a state-of-the-art coupled climate model with reasonable aerosol distributions (Ginoux et al., 2006) precomputed



offline through the chemical transport model MOZART-2 (Horowitz, 2006). CM2.1 contains a notably successful simulation of Earth's climate conditions over the past century (Knutson et al., 2006), and is adjudged to be a top tier model based on the climate metric examination by Reichler and Kim (2008). CM3 is the next generation climate model, in which aerosols fields are now calculated online with representations of gas-aerosol chemistry and aerosol-cloud interactions (Donner et al., 2011; Naik et al., 2013).

Aerosol parameters captured by the models include aerosol optical depth (AOD), scattering and absorption AOD, scattering extinction, and absorption extinction. We use these parameters to calculate single-scattering albedo (SSA) and the Ångström exponent ( $\alpha$ ). The Ångström exponent is a proxy of particle size that is derived from simultaneous wavelength measurements of AOD, and relies on the differential measurements to provide an indication of particle size. A smaller  $\alpha$  corresponds to larger particles, such as dust. A larger  $\alpha$  corresponds to smaller particles, such as black carbon. From analyzing data from 12 cities worldwide, Dubovik et al. (2002) show that  $\alpha$  is typically greater than 1 for urban-industrial and biomass burning particles, and typically less than 1 for dust particles. While the model computed extinction and optical depth in the visible and near-infrared wavelength bands, we focus our analysis on the visible wavelengths, which are taken to be 550 nm.

The main aerosol-related differences between CM2.1 and CM3 are (i) aerosols are computed offline in CM2.1 and online in CM3, (ii) emissions inventories are different, (iii) black carbon and sulfate are in external mixtures in CM2.1 and internal mixtures in CM3, and (iv) the injection height of biomass burning aerosols is included in CM3. CM3 also allows for aerosol-cloud interactions, but we do not consider those here. These changes introduce numerous variables that make determining discrepancies between the two models' aerosol properties challenging to quantify. Here we compare the aerosol optical properties from both models to form a thorough understanding what the discrepancies are, building on the initial comparisons provided by Donner et al. (2011) and Naik et al. (2013). More research is needed to parse out how each individual modification contributes to the changes in aerosol properties.

### 3.1 GFDL CM2.1

CM2.1 is a coupled atmosphere-ocean-sea ice-land global climate model (Delworth et al., 2006). The atmospheric component, developed by the GFDL Global Atmospheric Model Development Team (GAMDT) in 2004, has a horizontal resolution of  $2^\circ$  (latitude) by  $2.5^\circ$  (longitude), with 24 vertical levels; the top level is around 3 Pa. Aerosol fields are precomputed offline by the global three-dimensional chemical transport model Model for Ozone and Related Chemical Tracers (MOZART-2) (Ginoux et al., 2001; Horowitz et al., 2003; Tie et al., 2005; Horowitz, 2006), with distributions governed by emissions, chemical transformations (i.e. production of secondary aerosols and hygroscopicity), atmospheric transport (advection, diffusion, convection), and wet and dry deposition (Tie et al., 2005, Horowitz, 2006). The CM2.1 model then calculates the aerosol optical and radiative properties online.



Aerosols accounted for in MOZART-2 are sulfate, black carbon, primary organic carbon, secondary organic carbon, and mineral dust (five size bins based on Ginoux et al. (2001)). Aerosol and aerosol precursor emissions are taken from inventories compiled for IPCC Fourth Assessment Report (AR4), and present-day emissions are described in detail in Horowitz (2006). Anthropogenic sources include emissions from fossil fuel combustion, and biofuel and biomass burning.

5 The emissions database used here assumes no seasonality for fossil fuel combustion emissions. Biomass burning, on the other hand, is comprised of a seasonal cycle that is regionally dependent, but is climatological and does not vary year to year. Southern Hemisphere biomass burning sources peak in September-October-November, and Northern Hemisphere biomass burning sources peak in March-April-May. Natural sources, such as wind-driven sea spray and dust, biogenic and soil emissions, background volcanic degassing, and oceanic emissions, remain constant over time. Dust and sea salt emissions

10 are assumed to be entirely natural (Ginoux et al., 2001).

Black and organic carbon are emitted as 80% and 50% hydrophobic, respectively, the rest hydrophilic (Tie et al., 2005), and the hydrophobic compounds are converted into hydrophilic forms with a lifetime of 1.63 days (Reddy and Boucher, 2004). The precursor gas sulfur dioxide is oxidized to sulfate by hydroxyl radical in the gas phase and by hydrogen peroxide and ozone in the aqueous phase, with the reaction rates provided in Tie et al. (2001). Secondary organic carbon is formed via

15 oxidation of certain volatile organic compounds. Removal parameterizations for dry deposition, gravitational settling, and in-cloud and below-cloud wet scavenging are specified for each aerosol type, described in detail in Tie et al. (2005).

Aerosols are transported by advection, diffusion, and convection according to prescribed meteorological input fields. For all aerosols except dust, meteorological fields by the National Center for Atmospheric Research Community Climate Model (MACCM3) (Kiehl et al., 1998) were employed; dust was simulated separately using meteorological fields from the National

20 Centers for Environmental Prediction (NCEP)–National Center for Atmospheric Research (NCAR) Reanalysis (Kalnay et al., 1996). Sea-salt monthly concentrations are obtained from a previous study by Haywood et al. (1999). They have assumed a surface concentration proportional to the wind speed using the parameterization by Lovett (1978). Sea salt vertical concentration is assumed constant from the surface to 850 hPa, and zero above, and this distribution is kept constant over the years during the simulations (Ginoux et al., 2006).

25 Horizontal resolution of MOZART-2 is  $2.8^\circ$  by  $2.8^\circ$ , with 34 vertical layers extending up to 40 km (4 hPa). The model time step for chemistry and transport is 20 minutes. Three-dimensional monthly-mean decadal aerosol distributions are archived from MOZART-2 and remapped to the  $2^\circ$  by  $2.5^\circ$  resolution of CM2.1 with 24 vertical levels, and temporally interpolated. Aerosol surface concentrations derived by coupling MOZART-2 and CM2.1 have been thoroughly evaluated by Ginoux et al. (2006).

30 Aerosol optical depth, single scattering albedo, and asymmetry parameter are calculated from optical properties derived from Mie theory (Haywood and Ramaswamy, 1998) and the concentrations interpolated from MOZART-2 (except for sea salt,



which was prescribed following Haywood et al. (1999)). The aerosols are assumed to follow a lognormal size distribution (Haywood and Ramaswamy, 1998). Hygroscopic growth is considered for sulfate (as pure ammonium sulfate modeled after Tang and Munkelwitz (1994), using simulated relative humidity), and for sea salt (as pure sodium chloride (Tang et al., 1997), using a fixed relative humidity of 80%). In the radiative transfer code, black and organic carbon are assumed to remain dry, despite their hydrophilic properties taken into consideration for removal mechanisms in MOZART-2. While anthropogenic fossil fuel emissions of aerosols do not exhibit any seasonality, seasonal humidity generated within the model introduces a seasonal pattern to aerosol optical depths due to hygroscopic growth. Seasonality of aerosol distributions is also influenced by local meteorology.

For our analysis, we use aerosol parameters computed from a 5-member historical simulation ensemble where all forcings vary in time from 1860 to 2000. Five-year monthly mean averages from 1996-2000 are used to represent present-day. We build upon the analysis in Ginoux et al. (2006) that analyzed CM2.1 AOD at 102 AERONET sites and global coverage from satellite data (Moderate Resolution Imaging Spectroradiometer (MODIS)). Ginoux et al. found that CM2.1 aerosol distributions were often overestimated in polluted regions, and underestimated in biomass burning regions. In this study, we look at scattering and absorption AOD, scattering vertical extinction, absorption vertical extinction, single-scattering albedo, and the Ångström exponent in addition to overall AOD.

### 3.2 GFDL CM3

CM3 is GFDL's next generation coupled global climate model after CM2.1. Modifications to physics and dynamics are discussed in Donner et al. (2011). The horizontal domain was changed from a spherical grid to a standard  $6 \times 48 \times 48$  cubed-sphere grid, which is effective in avoiding convergence of grid cells at the poles. For reference, the grid boxes for the cubed-sphere framework at the equator are only slightly smaller than that of the Cartesian grid in CM2.1. The amount of vertical levels was doubled from 24 to 48 to better capture stratospheric chemical and dynamical processes, and the uppermost level increased from 3 Pa in CM2.1 to 1 Pa.

The aerosol treatment in CM3 is very different from CM2.1. First, emissions inventories are different. Second, aerosol distributions are computed online and interactive, such that the distributions are consistent with the model-generated meteorology. Third, aerosol-cloud indirect effects are enabled through the cloud-albedo and cloud-lifetime effects, and the wet deposition scheme is coupled to cloud microphysics (Donner et al. 2011). And fourth, sulfate and black carbon are assumed to be internally mixed for radiative calculations.

A modified version of MOZART-2 is inserted into CM3, simulating 97 chemical species, 16 of which are aerosols. Instead of using in-house emissions as in CM2.1 (Horowitz, 2006), the emissions in CM3 were provided by Lamarque et al. (2010), an inventory that was compiled for the Climate Model Intercomparison Project Phase 5 (CMIP5) in support of the Intergovernmental Panel on Climate Change (IPCC) Fifth Assessment Report (AR5). The emissions of aerosols in Lamarque



et al. (2010) are generally lower than that used in CM2.1 (see Table 1); present-day sulfur dioxide, black carbon, and dust emissions are considerably lower in CM3, while organic carbon is higher. As in emissions used for CM2.1, fossil fuel emissions of aerosols contain no seasonal variations. A key improvement to emissions in biomass burning regions are that the aerosols are vertically distributed, unlike in CM2.1, to more accurately capture the injection height of these aerosols. No information regarding elevation of biomass burning emissions was provided in the inventory, and thus the recommendations of Dentener et al. (2006) are followed to distribute emissions between the surface and 6 km.

As in CM2.1, black and organic carbon are emitted as 80% and 50% hydrophobic, respectively, the rest hydrophilic (Tie et al., 2005). However, the hydrophobic compounds are converted into hydrophilic forms with a lifetime of 1.44 and 2.88 days, respectively, a change from 1.63 days for both in CM2.1; the increase in lifetime of organic aerosols from hydrophobic to hydrophilic is based on experimental evidence in Huang et al. (2013), which uses a process-based aging scheme including the effects of chemical oxidation and physical condensation/coagulation. The treatments of chemistry and deposition are similar in CM2.1 and CM3 (Donner et al., 2011). Transportation of aerosols is similar overall, but there are differences in large-scale and subgrid transports that are responsible for some changes in aerosol fields. Recall that aerosols are now interactive within the meteorology of the model.

Aerosol optical property calculations (aerosol optical depth, single scattering albedo, and asymmetry parameter), size distribution assumptions, and refractive indices are unchanged from CM2.1 to CM3. Lognormal size distribution is assumed for sulfate and carbonaceous aerosols, also unchanged from CM2.1. However, hygroscopic growth was limited to 98% relative humidity in CM3 rather than 99.9% in CM2.1, as 99.9% was shown to produce excessive AOD in CM2.1 (Ginoux et al., 2006). Further, a key inclusion in CM3 is a globally pervasive internal mixing assumption that considers a homogenous mixture between sulfate, black carbon, and water by a volume-weighted average of their refractive indices. As in CM2.1, aerosol AOD exhibits seasonality in part due to the seasonal variation in local relative humidity, despite fossil fuel emissions not varying seasonally.

We use aerosol parameters computed from a 5-member historical simulation ensemble where all forcings vary in time from 1860 to 2005. Five-year monthly mean averages from 2000-2004 are used to represent present-day. We build upon the analyses in Donner et al. (2011) and Naik et al. (2013) that compared model-derived AOD to observations. Donner et al. (2011) found that while the emissions of black carbon are considerably decreased from CM2.1 to CM3 (Table 1), changes in AOD are partly compensated by increased absorption from internal mixing with sulfate. Further, reduced aerosol direct effects in CM3 led to increases in clear-sky downward shortwave radiation that were more consistent with observations, providing strong evidence that aerosol direct effects are better represented in CM3 than in CM2.1 (Donner et al., 2011). Naik et al. (2013) find that the mean bias of the CM3-simulated global aerosol optical depth is within 5% of satellite measurements over 1982 to 2004. Of the years in which volcanic aerosols in the atmosphere represents a minor contribution (1996 to 2006), the mean bias is within 2%. Overall, the improved AOD in CM3 is attributed mostly to changes in emissions



and the new internal mixing treatment (Donner et al., 2011). We extend these previous evaluations of model performance by expanding the amount of aerosol properties compared to observations, and also analyzing the vertical extinction distributions.

## 4 Results and discussion

### 5 4.1 Model aerosol properties

Fig. 2 shows a comparison between total aerosol optical properties simulated by the models – aerosol optical depth (AOD), aerosol absorption optical depth (AAOD), and single-scattering albedo (SSA), and Table 1 presents the global-mean values for the total optical depths. CM2.1 values are averages from 1996–2000, and CM3 values are averages from 2000–2004.

The applied emissions and resulting global aerosol burden in CM3 is significantly lower than that by CM2.1 (Naik et al., 2013). However, while sulfate and black carbon emissions and burdens are considerably lower in CM3, the overall aerosol optical depths (total, absorption, and scattering) are very consistent between the two models (Table 1). While reduced emissions and a lowered cap of relative humidity for sulfate hygroscopic growth yield a reduction in AOD in CM3, internal mixing of black carbon and sulfate introduced in CM3 produces higher AAOD than CM2.1, as explained by Persad et al. (2014). Further, organic carbon and sea salt global-mean optical depths have slightly increased from CM2.1 to CM3 (Fig. 3).

Further, while the global-mean AOD and AAOD are relatively consistent between the models, the spatial distributions show considerable differences. AOD and AAOD over Northeast U.S., Europe, and Australia source regions are much lower in CM3, whereas Brazil, Indonesia, and India show much higher AOD and AAOD in CM3. It is also clear that more scattering and absorbing aerosols are penetrating into the Arctic in CM3 than in CM2.1. The SSA plots show a higher SSA globally in CM3, (indicative of more scattering aerosols relative to absorbing), and particularly evident over Brazil and the Sahara desert.

Figure 3 breaks down the total AOD into individual components, and Table 1 provides global-mean emissions, burden, and optical depths for the major anthropogenic scattering and absorbing aerosol species, sulfate and black carbon, respectively. The individual aerosol AOD differences between CM2.1 and CM3 (Fig. 3) explain several regional differences seen in Fig. 2. Black and organic carbon biomass burning regions in South America, Africa, and Asia dominate their respective AODs in CM3, with North America and Europe playing minor roles. Sulfate is constrained in closer proximity to sources in CM3, yielding less diffusion of AOD in the Northern Hemisphere. Dust from the Sahara plays a slightly lesser role in CM3 than CM2.1 due to lower emission. Sea salt's regional pattern and magnitude is improved from the earlier version for which it was prescribed with constant value below 850 mb (Jaeglé et al., 2011).



Overall, attributions of aerosol species to total global-mean AOD are 5, 59, 6, 18, and 12% in CM2.1 for black carbon, sulfate, organic carbon, dust and sea salt, and 2, 43, 19, 11, 25% in CM3, respectively.

## 4.2 Comparisons of model data with observations

Datasets measured or derived from AERONET stations are useful in that they provide observations of various properties –  
5 such as aerosol optical depth (AOD), aerosol absorption optical depth (AAOD), single-scattering albedo (SSA), and the Ångström exponent ( $\alpha$ ). While studies often compare one or two parameters (e.g. Kinne et al., 2006), the availability of multiple parameters is valuable in evaluating aerosols in a model. Further, comparing AERONET column data with collocated aerosol profile observations (from CALIOP) can provide insight into the vertical structure of extinction, which is also simulated by models.

### 10 4.2.1 Evaluating multiple aerosol parameters

Comparisons of the five-year averages of model data (CM2.1 and CM3) with averages of all available AERONET data are found in Figs. 4 (polluted cities) and 5 (biomass burning regions). Aerosol parameters compared include AOD, scattering AOD, AAOD, SSA, and  $\alpha$ . The error bars for the AERONET data represent year-to-year variability in the available data.

Overall, compared to AERONET data, the CM2.1 model slightly overestimates AOD in Oklahoma, overestimates AOD in  
15 Belsk, underestimates AOD in Kanpur, slightly underestimates AOD in Taiwan, and underestimates AOD in all biomass burning sites (Alta Floresta, Mongu, Mukdahan). CM3 reasonably reproduces the AOD magnitudes in Oklahoma, Belsk, Kanpur, and Mukdahan, although the seasonality of AOD (derived by humidity influence on optical depth as opposed to emissions) is weakly captured by CM3, even for biomass burning regions that do contain seasonality in their emissions inventories. Both models consistently reproduce the magnitudes and seasonality of single-scattering albedo and the  
20 Ångström exponent, with CM3 showing great improvements in some (e.g. Belk  $\alpha$ ; Alta Floresta SSA), and a downgrade in others (e.g. Taiwan, Kanpur, Alta Floresta, Mongu, Mukdahan  $\alpha$ ).

The site in Oklahoma is in a rural environment compared to the other urban sites we have chosen for model evaluation, and therefore total AOD is considerably lower. The largest nearby cities are Wichita, Kansas; Tulsa, Oklahoma; and Oklahoma City, Oklahoma; and each is at least 100 km away. Pollution sources may be heavy industries in Texas cities such as  
25 Houston and Dallas, while dust from the southwest U.S. and northern Mexico, and possibly long-range transport of dust from Asia (VanCuren and Cahill, 2002; Andrews et al., 2011) could also be causal factors. Air mass back-trajectories show that summertime air originates in polluted regions of Texas, while wintertime air is from cleaner, northern sources (Andrews et al., 2011).



Both CM2.1 and CM3 reproduce the AOD (total, scattering, and absorption), SSA, and  $\alpha$  magnitudes to well within a factor of two (Fig. 4). The seasonality is not well represented, but is better in CM3. AERONET shows an Oklahoma AOD maximum in May and August, while CM2.1 derives peaks in April and September attributable to high sulfate AOD (not shown). AERONET, CM2.1, and CM3 all show AOD minimums from October to February. The models and AERONET  
5 both show a drop in  $\alpha$  during springtime reaching a minimum in April, which is indicative of the presence of dust, and a rebound in summer attributed to the peaks in sulfate.

CM2.1 AOD is considerably overpredicted in Belsk by a factor of three or more from April to September. Upon further investigation, this is partly attributed to Poland's shift to a market economy in 1990 that has since steadily reduced pollution emissions (The World Bank, 2011) and partly attributed to the economic crash of 2008, not considered in the model. The  
10 discrepancy may thus be attributed to a mismatch of periods between the model and AERONET. CM3, however, represents the AOD magnitudes in Belsk much better.

AERONET shows one peak in April, and another in July–August. CM2.1 reasonably reconstructs the seasonality with a slight peak in AOD in April, slight dip May to June, and then slight peak again in July to September, whereas CM3 only has one peak in June. Analysis of back-trajectories computed using the NOAA HYSPLIT model and fire maps show that these  
15 peaks coincide with seasonal biomass burning in eastern and southern Europe (Jaroslowski and Pietruczuk, 2010). Another study uses LIDAR measurements and model results to suggest that transport of Saharan dust also influences springtime AOD in Belsk (Pietruczuk and Chaikovsky, 2012). This is consistent with CM2.1 (and not CM3), which shows a maximum absorption AOD, minimum SSA, and minimum Ångström exponent during March–April–May, as well as a peak in the dust AOD in May.

For Kanpur, peaks in AOD during May and October are partly associated with peaks in open biomass burning of rabi and kharif agricultural crops, respectively (Venkataraman et al., 2006). There is also a significant enhancement in dust loading during the pre-monsoon season (April to June) (e.g., Ginoux et al., 2012). Post-monsoon, aerosols transported to or emitted near Kanpur can accumulate rapidly in the atmosphere from suppressed precipitation (Dey and Di Girolamo, 2010). Monthly emissions from fossil fuel and biofuel combustion are fairly constant (Reddy and Venkataraman, 2002). Dey and Di  
20 Girolamo (2010) analyzed nine years (2000–2008) of AOD seasonal climatology derived from the MISR – an instrument aboard the NASA Terra spacecraft – and the results are consistent with those shown by AERONET. Dey and Di Girolamo (2010) used air mass back trajectories – calculated using the NOAA HYSPLIT model – to show that the Great Indian Desert and the Arabian Peninsula are the likely sources of the dust.

CM2.1 AOD is consistently underpredicted in Kanpur by a factor of four on average, but this is expected because Kanpur  
30 has incredibly high pollution levels of which models with the resolutions of CM2.1 and CM3 are not expected to resolve. CM3 does, however, have better magnitudes. The CM2.1 and CM3 maximum AOD coincides with a minimum AOD as



measured by AERONET during the monsoon season (July to September). Likewise, the CM2.1 and CM3 minimum AOD coincides with a maximum AOD as measured by AERONET during the dry season (October to January). The presence of high AOD in the winter months is verified by several satellite instruments including CALIOP (Cloud–Aerosol Lidar with Orthogonal Polarization), MODIS (Moderate Resolution Imaging Spectroradiometer), MISR (Multiangle Imaging Spectroradiometer), OMI (Ozone Monitoring Instrument), and TOMS (Total Ozone Mapping Spectrometer) (Ganguly et al. (2009b) and references therein).

Emissions inventories in India have large uncertainties (Venkataraman et al., 2006), and because both CM2.1 and CM3 do not prescribe any seasonality in emissions from anthropogenic sources, it is unsurprising that the chemistry–transport or chemistry–climate models cannot reconstruct Kanpur’s AOD seasonal climatology,. Ganguly et al. (2009b) found that a decoupled version of the model used here (GFDL AM2) largely underestimated carbonaceous aerosols in the Kanpur region by as much as a factor of 10 during winter months. The high summer bias in Kanpur AOD during the summer months is likely due to convective removal of aerosols simulated too low, therefore leading to high biases especially in the tropics where convective large scale precipitation is dominant (Paulot et al., 2015). Further, in addition to dust transport from desert regions, anthropogenic sources of dust are prevalent in India from agricultural activities and land use (Ginoux et al., 2012). This is also not accounted for in CM2.1.

SSA observations are much lower in Kanpur as compared to the other sites (~0.88 compared to ~0.92–0.98), which is representative of its relatively large black carbon and dust concentrations. Kanpur also has the smallest  $\alpha$  of the four sites. Both model shows this as well. Kanpur  $\alpha$  is consistent with the observation that the pre-monsoon aerosol loading includes a large dust component. While CM2.1 underestimates AOD in Kanpur and does not simulate the seasonal climatology, the absorption AOD and  $\alpha$  suggest that dust particles are present in the model from March to May. CM3 overpredicts  $\alpha$  in Kanpur, perhaps showing too little dust.

Aerosols in Taiwan have industrial, biomass burning, and dust storm sources. The region is highly polluted from nearby heavy industries year-round (Chen et al., 2009). Springtime aerosols in Taiwan and Southeast Asia are partly attributed to intense dust storms in Mongolia and North China, which have been observed to travel in the mid-troposphere all the way to Europe (Grousset et al., 2003), and have also been observed at lower latitudes in Taiwan (Chen et al., 2009; Wong et al., 2013). Peak biomass burning season in Southeast Asia also occurs during the spring (Streets et al., 2003). CM2.1 somewhat captures the March–April peak, although CM3 shows a peak during summer months where AOD is at a minimum; this may also be due to the low convective removal of aerosols leading to high biases in the tropics (Paulot et al., 2015). CM2.1 also accurately captures the October–November peak and summertime minimum, whereas CM3 does not.

Both the dust, and carbonaceous aerosols from biomass burning, likely contribute to a drop in the SSA during the springtime months (seen in AERONET and models), although dust is more absorbing in the near-UV than in the visible spectrum



whereas the opposite is true for black carbon. The lack of a drop in  $\alpha$  derived from AERONET during spring likely represents the balancing out of more large particles (dust) and more fine particles (black and organic carbon).

In autumn, air mass back trajectories computed by Chen et al. (2009) using the NOAA Hybrid Single Particle Lagrangian Integrated Trajectory Model (HYSPLIT) model show variable sources including northwest China, southern China, and the  
5 Pacific Ocean. Therefore, it is hard to attribute the cause of the secondary peak in AOD during October–November.

Overall, CM2.1 and CM3 reproduce AOD magnitudes fairly well, and CM2.1 actually captures the seasonality reasonably. The single-scattering albedo and Ångström exponent are also well-simulated for all four industrialized cities, despite any inconsistencies with AOD. Using CM2.1 dust and black carbon absorption AOD as a proxy for concentrations, peaks in  
10 CM2.1 dust absorption AOD are correlated well with dips in the AERONET  $\alpha$ , and peaks in CM2.1 black carbon absorption AOD are correlated well with peaks in the AERONET  $\alpha$  (not shown).

The model suggests that, for the industrialized sites, the total and scattering AODs are dominated by sulfate, and absorption AOD is dominated by black carbon with a significant contribution from dust (not shown). Organic carbon, and sea salt especially, play minor roles at most. However, Heald et al. (2005) suggest that global climate models underestimate the contribution of organic carbon to the total aerosol concentration and AOD. In particular, Ganguly et al. (2009a) suggest that  
15 sulfate concentrations are overestimated and organic concentrations are underestimated in CM2.1 over Oklahoma.

For the biomass burning regions (Fig. 5), the models' AOD are much less consistent with the AERONET observations during burning season. CM2.1 consistently underpredicts total AOD by a factor of 4–6 during peak biomass burning emissions (September for Alta Floresta and Mongu, and March for Mukdahan). CM3 shows similar results for Alta Floresta and Mongu, but with a huge spike in Mukdahan AOD during June through September that rivals March magnitudes, a time  
20 when AOD is at a minimum according to AERONET.

Underestimations during peak biomass burning season may be due to underestimated emissions, an injection height that is too low, efficient wet removal in convective regions, and/or the lack of hygroscopic growth of carbonaceous aerosols. The severe underestimates in biomass burning aerosols in the models could impact model-derived climate changes important to understanding aerosol's role in climate change, due to the lack of aerosols in the Southern Hemisphere which would play a  
25 role in cross-equatorial energy balance (Ocko et al., 2014).

Although AOD are underestimated during peak biomass burning season, there is a slight peak in model AOD (with the exception of Mukdahan) suggesting that the model does capture the seasonal cycle of biomass burning, just not the scale of the emissions or concentrations. The models do, however, capture a secondary peak in Mukdahan emissions in September–October, and the AOD magnitudes are consistent as well. When it is not biomass burning season in any of these regions,



CM2.1 is consistent with AERONET observations, although CM3 shows higher AOD from December through March in Alta Floresta and Mongu that has no parallel in the AERONET Data.

Alta Floresta AERONET AOD maxima are the highest of any comparison site analyzed in this study. As shown in Fig. 5, AOD during the main biomass burning season in Alta Floresta (August to September) has high year-to-year variability, and the average AOD from 1993–2012 in September is almost 1.5. In fact, Hoelzemann et al. (2009) found that Alta Floresta had the highest AOD observed (4.0) of all 12 observation sites the study analyzed in South America using MODIS satellite data. The large AOD is due to intense fire activity that exists in the vicinity of Alta Floresta due to deforestation. Prior to August, during the dry season, climatological patterns in central Brazil may efficiently dilute pollution by exporting it to the ocean (Freitas et al., 2009).

Over Alta Floresta, AERONET derives a SSA for July through December of approximately 0.95. CM2.1 projects a sharp decline in SSA during these months that drops to 0.8, but CM3 brings the magnitudes back up closer to observations. While absorption AOD in the models is only underestimated by a factor of 2 in Alta Floresta during peak emissions (September), scattering AOD is underestimated by more than 4 times. This means that the model accounts for more absorption relative to scattering than is actually present, yielding low SSA. A larger scattering AOD would yield SSA closer to 1. The Ångström exponent derived by AERONET is consistent with CM2.1, and shows a drop in  $\alpha$  from January to May; CM3 also shows this pattern, but overestimates the amount of smaller particles. During peak fire activity, however,  $\alpha$  is considerably higher. There is also large year-to-year variability in  $\alpha$  in Alta Floresta.

Maximum seasonal AOD in Mongu as measured by AERONET from 1995 to 2010 is half that of Alta Floresta (0.8). Tropical Africa is characterized by widespread and frequent forest fires that occur consistently each year. MODIS satellite data show that burning begins in May and peaks July to September (Giglio et al., 2003, 2006). This is slightly shifted from AERONET AOD data, which show maxima between August and October. The apparent offset between MODIS fire activity and AERONET AOD is corroborated by aircraft data analyzed in Magi et al. (2009), which shows a shift in peak AOD by 1–2 months after peak fire activity. CM2.1 and CM3 show slight increases in AOD that align in timing with AERONET, although CM3 has an additional peak in February which is not shown in the observations.

As mentioned earlier, the models capture one of the two AERONET AOD maxima over Mukdahan. Mukdahan is influenced by nearby crop and vegetation burning and wildfires throughout the dry season; biomass burning activity first peaks in March, with a second, smaller peak in autumn after the rainy season (Boonjawat, 2008). The February to April peak evident in AERONET in fact corresponds to a decrease in model AOD. The September–October peak, on the other hand, is well captured by CM2.1 in both timing and magnitude. The springtime AOD in the observations is considerably higher than that in autumn, which may be a result of changes in burning conditions (wildfire vs. controlled burn) and vegetation type (Dubovik et al., 2002). Concurrently, the AERONET data show a drop in SSA and a peak in  $\alpha$  that is extremely consistent



with the models and suggestive of carbonaceous particles from burning. Because of the lack of moisture during the winter dry season, the peak in  $\alpha$  may also be attributed to the lack of hygroscopic growth (Logan et al., 2013). The models also show a slight increase in dust AOD during summer in Mukdahan (not shown), which matches up well with a sharp dip in AERONET  $\alpha$ .

- 5 Overall, model AOD magnitudes are more consistent with AERONET observations in industrialized areas than for biomass burning areas, although the model reproduces satisfactorily SSA and  $\alpha$  at most sites. Model AOD magnitudes in biomass burning regions are less consistent with the AERONET observations, and maximum AOD are underestimated in the model by as much as factors of 4 to 6. While CM2.1 captures the seasonality for AOD for most locations, CM3 shows peaks when there are minimums.

#### 10 4.2.2 Evaluating model-derived data with collocated instruments

Whereas AERONET provides a two-dimensional view of aerosol properties via total column estimates, CALIOP measurements provide insight into the vertical structure of the aerosol properties, revealing the elevations of aerosols. This is incredibly important and useful for climate model evaluation because aerosol radiative effects are extremely sensitive to elevation (e.g. Ocko et al., 2014). Satellite measurements are further valuable because they have a broad spatial coverage.

- 15 Here we weave in the CALIOP data to the existing AERONET/model discussion. Figs. 6 and 7 compare the seasonal CALIOP measurements at 532 nm to the models' estimates (at 550 nm) for the industrialized and biomass burning sites, respectively.

As discussed earlier, while CM3 decently captures the AERONET AOD seasonality for Oklahoma, CM2.1 captures the vertical structure of the seasonality when looking at the vertical distribution of extinction. On the other hand, CM3 does not exhibit two distinct seasonal peaks at higher elevations as shown in both the CALIOP and CM2.1 data. This highlights the need for comparing model data to multiple observational datasets.

- 20
- For Belsk and Taiwan, the CM2.1 reasonably reproduces the seasonality and elevations of extinction well, although surface extinctions are overestimated at both sites. CM3 does a better job with surface extinction magnitudes in Belsk and Taiwan. As discussed previously, emissions in eastern Europe were considerably reduced as a result of switching economic regimes as well as subsequent economic stress from the crash of the world economy.

Belsk maxima AOD are slightly offset from AERONET data (March instead of April, October–November instead of August–September). However, AERONET does show a peak in absorption AOD in March with high year-to-year variation (large error bar), as well as a drop in both SSA and  $\alpha$ . This is consistent with conclusions by Pietruczuk and Chaikovsky (2012) that dust is transported to Europe from the Saharan desert during spring. Overall, AERONET AOD and CALIOP extinction are consistent with one another, and well below what the CM2.1 model suggests; CM3 does a better job.

- 30



For Taiwan, AERONET suggests higher AOD than CALIOP. As compared to AERONET data, the model correctly reproduces magnitudes of AOD and slightly underestimates the springtime maxima. However, the CM2.1 model's vertical extinction profile is considerably larger than that of CALIOP. The springtime AOD from AERONET and the extinction vertical profile from CALIOP emphasize the importance of the vertical distribution of aerosols in the atmosphere. While the springtime AOD peak in AERONET is slightly larger than the peak in autumn, CALIOP shows large differences in the vertical distribution of extinction during spring and autumn. During springtime, aerosol extinction reaches higher elevations than during autumn. This is consistent with studies showing long-range high-elevation transport of dust (Lin et al., 2007), and also consistent with ground-based LIDAR measurements in Taiwan (Chen et al., 2009). Recall that the main springtime sources of aerosols in Taiwan (other than industry) are dust transported from the north, and nearby biomass burning. During autumn, high extinctions are constrained closer to the ground. Interestingly, the total column optical depth when computed from CALIOP data show that the overall AODs are similar for spring and autumn, even though their vertical distributions vary tremendously. This shows the value of instruments like CALIOP in their ability to resolve aerosol vertical profiles. The model, on the other hand, does not accurately distinguish the differences in the vertical profiles over Taiwan, and springtime and autumn extinction distributions are fairly comparable.

For Kanpur, both models capture the fall peak but not the spring peak. However, CM2.1 underestimates the magnitude and elevation of extinction, whereas CM3 does a much better job. As discussed in Sect. 3.2.1.1, the wintertime and pre-monsoon seasons are largely influenced by enhanced dust loading from nearby deserts, and agricultural and land use activities (Ginoux et al., 2012). While the CM2.1 model accounts for natural sources of dust, and captures a slight peak in dust emissions during this period (Fig. 4), it does not account for anthropogenic sources. It is very likely that CM2.1 also underestimates concentrations of carbonaceous aerosols from biomass burning in this region during these seasons. On the other hand, AERONET and CALIOP show the same seasonal trends, except that AERONET AOD remains high during winter months whereas CALIOP extinction drops from November to February.

Fig. 7 compares the seasonal CALIOP measurements at 532 nm to the model estimates (at 550 nm) for the biomass burning sites. Extinction seasonality shown by CALIOP is consistent with AERONET AOD, with maximum extinction during September in Alta Floresta and Mongu, and March/September–October for Mukdahan. It is clear from the CALIOP data that aerosols reach much higher elevations over biomass burning influenced sites as compared to industrialized sites; the strongest extinctions can extend up to 3 km in the atmosphere.

As suggested by Fig. 5 in the AERONET comparisons, CM2.1 and CM3 completely miss the large magnitudes of extinction during biomass burning seasons, with the exception of Mukdahan in the fall. However, the models do somewhat capture the seasonal cycles at all three sites, but the extinctions are completely underestimated by a factor of 10. Higher extinction magnitudes are also constrained closer to the surface in the models, whereas in reality, and as shown by CALIOP, aerosols from biomass burning sources can be lofted high into the atmosphere.



In CM2.1, carbonaceous aerosols from biomass burning are emitted from the surface (Horowitz, 2006). However, because it has been known for quite some time that injection height from open fires and wet deposition are key to simulating smoke plumes properly (e.g., Westphal and Toon, 1991), biomass burning emissions for CM3 were distributed vertically. As discussed before, aerosols in the boundary layer have a relatively short lifetime due to efficient dry deposition at the surface  
5 by the turbulent boundary layer, while aerosols injected into the mid- or upper troposphere can be transported over very long distances. Our results show that CM3 likely needs to increase the vertical structure for the biomass burning emissions, because particles are still not distributed high enough when compared to CALIOP data.

Other factors that may contribute to the underestimate in concentrations over biomass burning regions are underestimated emissions, too much wet removal in convective areas, the ratio of hydrophilic to hydrophobic aerosols, vertical mixing  
10 (convection), and hygroscopic growth of carbonaceous aerosols.

Overall, comparing the models vertical profiles of extinction with CALIOP data for all seven sites shows that seasonality is reproduced much better than the magnitudes and elevations of extinction, both of which are controlled by meteorology and emissions in the case of biomass burning sites. It is interesting that the models can reproduce seasonality in industrialized regions when emissions do not have a prescribed seasonal distribution. For biomass burning sites in particular, which are  
15 controlled by emissions inventories, seasonal maxima are consistent, however, the extent and height of aerosols in the atmosphere is severely underestimated (except for Mukdahan in late summer). This problem may be attributed to a combination of factors, such as the lack of modeling of the injection height of particles from open fires (and therefore efficient removal in the turbulent boundary layer), underestimated emissions, or excess wet removal of aerosols in convective regions. AERONET and CALIOP measurements are fairly consistent with one another, and show similar  
20 seasonal patterns.

## 5 Conclusions

We have compared several aerosol optical properties from two measurement techniques – ground-based sun photometers (AERONET) and satellite LIDARs (CALIOP) – to aerosol properties derived from two state-of-the-art climate models. We chose seven sites with long-term time series of AERONET measurements (at least seven years, at most 19 years) as a basis  
25 for our comparison, specifically selecting sites with industrial and biomass burning sources of aerosols. The sites include an urban-influenced rural area in Oklahoma, USA, with industrial and dust sources; Belsk, Poland, with industrial and dust sources; Kanpur, India, with industrial, dust, and biomass burning sources; Taiwan with industrial, dust, and biomass burning sources; Alta Floresta, Brazil with biomass burning sources; Mongu, Zambia, with biomass burning sources; and Mukdahan, Thailand, with biomass burning sources. We have also compared our results to several previous studies –  
30 modeling, observational, or both – for each comparison site.



Compared to the different observational datasets, the CM2.1 model overestimates (<50%) aerosol optical depth (AOD) in Oklahoma, overestimates (300%) AOD in Belsk, underestimates (100%) AOD in Kanpur, underestimates (<50%) AOD in Taiwan, and considerably underestimates (by a factor of four) the peak AOD magnitude and vertical extent at all biomass burning sites (Alta Floresta, Mongu, Mukdahan). The CM3 model, with improved aerosol treatment, does a better job in reproducing optical depth/extinction magnitudes as compared to CM2.1, as found in Donner et al. (2011), but a worse job with recreating seasonality, which is reproduced reasonably by CM2.1 despite the fact that the majority of emissions are aseasonal. Both models do a very nice job reproducing single-scattering albedo and the Ångström exponent, indicative of the types of aerosols present, with few exceptions.

Comparing multiple aerosol optical properties derived by models to measurements from collocated instruments both identifies opportunities for the improvement of modeling aerosol distributions, as well as reveals important aspects governing aerosol properties.

Key findings in this study include:

- All of the aerosol optical parameters in models should be evaluated against available observations in order to validate the model's credibility, as one parameter can reproduce satisfactorily the observations while another totally fails. This was demonstrated in Sect. 4.2.1, where for seven cities worldwide, the models accurately reproduced single-scattering albedo and the Ångström exponent, but under- or overestimated aerosol optical depth.
- Comparing AERONET data with CALIOP data shows the importance of measuring the vertical distribution of aerosols in the atmosphere. For example, while AERONET data shows that total AOD in February to May and September to November in Taiwan are similar, the CALIOP data reveals that the vertical distribution of the extinctions are considerably different during these two seasons. The difference in vertical distributions also provides insight into the origins of the aerosol particles in the atmosphere. For instance, dust sources originating from northern Asia may be transported at higher elevations in the atmosphere, whereas local pollution is generally constrained closer to the surface.
- Improvements to the modeling of aerosols originating from biomass burning sources involve increasing the injection height of biomass burning particles to avoid rapid removal by near-surface turbulence and therefore more properly represent the vertical profile of these species. Sect. 4.2.2 showed that model extinction vertical profiles over biomass burning regions, even in CM3 which accounted for the injection height, were too low as compared to AERONET and CALIOP data.



- Finally, analyzing aerosol properties derived from two related, but distinctly different global climate models is important in further determining how to improve the physics of the models for future versions. While further analysis is needed to pinpoint exactly how to improve the aerosol treatment in this model lineage, what is clear is that while some aspects have been drastically improved in the newer version CM3 (such as extinction magnitude and elevation) other aspects are worse than before (such as seasonality).

5

The comparisons of CM2.1 and CM3 aerosol properties to different observational datasets at four polluted cities and three biomass burning regions highlight model radiative forcing biases. It is evident that for almost all biomass burning regions, the models underpredict AOD and the vertical extent of aerosols in the atmosphere; we therefore expect that the radiative forcing by carbonaceous aerosols in these regions are also underestimated, and the positive radiative forcing from black carbon is biased too low due to (i) less overall mass of black carbon, and (ii) lack of black carbon forcing amplification from being located above clouds (e.g. Ocko et al. 2012).

10

AOD (and particularly scattering AOD) over industrialized areas provides a mixed picture in terms of biases; some sites have accurate reconstructions by the models, and others are largely over- (e.g. Belsk in CM2.1) or underestimated (e.g. Kanpur in CM2.1). Therefore, there may be compensating AOD biases over the globe that lead to the canceling out of associated biases in the sulfate radiative forcing over large domains, but the biases may affect the regional distribution of forcing. On the other hand, the models do a fairly reasonable simulation of the seasonality (though this is not the case for CM3), single-scattering albedo, and particle size in all seven locations, leading to few biases in these properties. Because CM3 meteorology was interactive with aerosols, as opposed to CM2.1 where aerosol distributions were computed offline, CM3 needs more analysis into the dynamical feedbacks that generate aerosol seasonality from emissions data that lack seasonality.

15  
20

Model biases in AOD may also perturb the interhemispheric forcing asymmetry, which directly impacts climate (Ocko et al., 2014). For example, if black carbon AOD in biomass burning regions (many of which are located in the Southern Hemisphere in Africa and South America) are largely underestimated, we would expect the radiative forcing to also be underestimated in these areas. Accounting for this underestimate would yield a higher black carbon radiative forcing in the Southern Hemisphere, and therefore less interhemispheric forcing asymmetry during peak biomass burning season. Because the majority of sulfate is located in the Northern Hemisphere, we do not expect a similar bias in the sulfate interhemispheric forcing asymmetry, which is more certain and already more pronounced than that of black carbon.

25

Model biases in organic carbon must also be considered. The formation of secondary organics is poorly understood, and carbonaceous material from non-fossil fuel combustion has poor emissions databases (e.g., biofuel combustion, cowdung burning, tea leaves burning). Organic carbon concentrations are likely too low in the models in biomass and biofuel burning regions. If the scattering by organic carbon is dominant, the underestimate may cancel out some of the bias in the

30



underpredicted black carbon forcing in these regions, thereby retaining the stark interhemispheric forcing asymmetry exhibited by black carbon. If, on the other hand, the absorption by organic carbon is dominant, correcting this bias would further amplify the positive forcing in these areas, leading to an additional reduction in the interhemispheric forcing asymmetry.

- 5 Overall, the model biases revealed by comparisons of model data to collocated observations may affect the interhemispheric aerosol forcing asymmetry, regional magnitudes of the forcings, and the seasonality of the forcings. However, when comparing model optical properties with measurements, it is also important to account for uncertainties in the aerosol optical properties derived from instruments, discussed in Sect. 2.2.

10 Finally, only recently tri-dimensional compositions of aerosols are being retrieved from sun photometers and LIDAR measurements (Chaikovsky et al., 2016), algorithms have been developed to tease out the individual aerosol components from datasets produced by AERONET, MPLNET, and CALIOP (Ganguly et al., 2009a, 2009b). This is especially useful for model validation of specific aerosol components, such as strong scatterers and absorbers – sulfate and black carbon – that significantly alter the Earth’s radiation budget from human activity and are an important, albeit uncertain, aspect of climate modeling.

## 15 Acknowledgements

We would like to thank the NOAA GFDL CM2.1 and CM3 model developers, and especially Larry Horowitz for running the CM3 simulations. We also thank the entire Cloud-Aerosol Lidar and Infrared Pathfinder Satellite Observation (CALIPSO) science team for providing CALIOP data, and the principal investigators and site managers of the seven AEROET stations that we acquired data from. We are grateful to Vaishali Naik for providing helpful comments on the  
20 manuscript.

## References

- Andrews, E., Sheridan, P. J., and Ogren, J. A.: Seasonal differences in the vertical profiles of aerosol optical properties over rural Oklahoma, Atmos. Chem. Phys., 11, 10661-10676, doi:10.5194/acp-11-10661-2011, 2011.
- 25 Bollasina, M. A., Ming, Y., and Ramaswamy, V., Anthropogenic aerosols and the weakening of the South Asian summer monsoon, Science, 334, 502-505, doi:10.1126/science.1204994, 2011.
- Bond, T. C., Doherty, S. J., Fahey, D. W., Forster, P. M., Berntsen, T., DeAngelo, B. J., Flanner, M. G., Ghan, S., Kärcher, B., Koch, D., Kinne, S., Kondo, Y., Quinn, P. K., Sarofim, M. C., Schultz, M. G., Schulz, M., Venkataraman, C., Zhang, H., Zhang, S., Bellouin, N., Guttikunda, S. K., Hopke, P. K., Jacobson, M. Z., Kaiser, J. W., Klimont, Z., Lohmann, U.,



- Schwarz, J. P., Shindell, D., Storelvmo, T., Warren, S. G., Zender, C. S.: Bounding the role of black carbon in the climate system: a scientific assessment, *J. Geophys. Res.*, 118, 5380-5552, DOI: 10.1002/jgrd.50171, 2013.
- Boonjawat, J.: Impact Assessment of Biomass-burning Aerosols in Southeast Asia, Greater Mekong Subregion – Core Environmental Program Capacity Development Workshop: Regional Air Pollution, Royal Princess Hotel, Bangkok, Thailand, <http://www.atm.ncu.edu.tw/95/ppt/>, 8–10 October 2008.
- 5 Boucher, O., Randall, D., Artaxo, P., Bretherton, C., Feingold, G., Forster, P., Kerminen, V.-M., Kondo, Y., Liao, H., Lohmann, U., Rasch, P., Satheesh, S.K., Sherwood, S., Stevens, B., and Zhang, X.Y.: Clouds and Aerosols. In: *Climate Change 2013: The Physical Science Basis. Contribution of Working Group I to the Fifth Assessment Report of the Intergovernmental Panel on Climate Change* [Stocker, T.F., Qin, D., Plattner, G.-K., Tignor, M., Allen, S.K., Boschung, J., Nauels, A., Xia, Y., Bex, V., and Midgley, P.M. (eds.)]. Cambridge University Press, Cambridge, United Kingdom and New York, NY, USA, 2013.
- Brasseur, G. P., Hauglustaine, D. A., Walter, S., Muller, J. F., Rasch, P., Granier, C., and Tie, X.: MOZART: A global three-dimensional chemical-transport-model of the atmosphere, *J. Geophys. Res.*, 103, 28,265 – 28,289, 1998.
- Chaikovskiy, A., Dubovik, O., Holben, B., Bril, A., Goloub, P., Tanré, D., Pappalardo, G., Wandinger, U., Chaikovskaya, L., Denisov, S. and Grudo, J.: Lidar-Radiometer Inversion Code (LIRIC) for the retrieval of vertical aerosol properties from combined lidar/radiometer data: development and distribution in EARLINET. *Atmos. Meas. Tech.*, 9, 1181-1205, 2016.
- 15 Chen, W.-N., Chen, Y.-W., Chou, C. C. K., Chang, S.-Y., Lin, P.-H., and Chen, J.-P.: Columnar optical properties of tropospheric aerosol by combined lidar and sunphotometer measurements at Taipei, Taiwan, *Atmos. Environ.*, 43, 17, 2700–2708, doi:10.1016/j.atmosenv.2009.02.059, 2009.
- Cooke, W. F. and Wilson, J. J. N.: A global black carbon aerosol model, *J. Geophys. Res.*, 101, 19,395 – 19,409, 1996.
- Delworth, T. L., Broccoli, A. J., Rosati, A., Stouffer, R. J., Balaji, V., Beesley, J. A., Cooke, W. F., Dixon, K. W., Dunne, J., Dunne, K. A. and Durachta, J. W: GFDL's CM2 global coupled climate models. Part I: Formulation and simulation characteristics, *J. Climate*, 19(5), 643-674, 2006.
- Dentener, F., Kinne, S., Bond, T., Boucher, O., Cofala, J., Generoso, S., Ginoux, P., Gong, S., Hoelzemann, J.J., Ito, A. and Marelli, L.: Emissions of primary aerosol and precursor gases in the years 2000 and 1750 prescribed data-sets for AeroCom, *Atmos. Chem. Phys.*, 6(12), 4321-4344, 2006.
- 25 Dey, S. and Di Girolamo, L.: A climatology of aerosol optical and microphysical properties over the Indian subcontinent from 9 years (2000–2008) of Multiangle Imaging Spectroradiometer (MISR) data, *J. Geophys. Res.*, 115, D15, doi:10.1029/2009JD013395, 2010.
- Donner, L. J., Wyman, B. L., Hemler, R. S., Horowitz, L. W., Ming, Y., Zhao, M., Golaz, J. C., Ginoux, P., Lin, S. J., Schwarzkopf, M. D. and Austin, J.: The dynamical core, physical parameterizations, and basic simulation characteristics of the atmospheric component AM3 of the GFDL global coupled model CM3, *J. Clim.*, 24(13), 3484-3519, 2011.
- Dubovik, O., Holben, B. N., Eck, T. F., Smirnov, A., Kaufman, Y. J., King, M. D., and Slutsker, I.: Variability of absorption and optical properties of key aerosol types observed in worldwide locations, *J. Atmos. Sci.*, 59, 590 – 608, 2002.



- Dubovik, O. and King, M. D.: A flexible inversion algorithm for retrieval of aerosol optical properties from Sun and sky radiance measurements, *J. Geophys. Res.*, 105, 20 673-20 696, 2000.
- Dubovik, O., Sinyuk, A., Lapyonok, T., Holben, B. N., Mishchenko, M., Yang, P., Eck, T. F., Volten, H., Munoz, O., Veihelmann, B., van der Zande, W. J., Leon, J.-F., Sorokin, M., and Slutsker, I.: Application of spheroid models to  
5 account for aerosol particle nonsphericity in remote sensing of desert dust, *J. Geophys. Res.*, 111, doi:10.1029/2005JD006619, 2006.
- Dubovik, O., Smirnov, A., Holben, B. N., King, M. D., Kaufman, Y. J., Eck, T. F., and Slutsker, I.: Accuracy assessments of aerosol optical properties retrieved from Aerosol Robotic Network (AERONET) Sun and sky radiance measurements, *J. Geophys. Res.*, 105(D8), 9791–9806, doi:10.1029/2000JD900040, 2000.
- 10 Feichter, J., Kjellström, E., Rodhe, H., Dentener, F., Lelieveld, J., and Roelofs, G.: Simulation of the tropospheric sulfur cycle in a global climate model, *Atmos. Environ.*, 30, 1693 – 1707, 1996.
- Freitas, S. R., Longo, K. M., Silva Dias, M. A. F., Chatfield, R., Silva Dias, P., Artaxo, P., Andreae, M. O., Grell, G., Rodrigues, L. F., Fazenda, A., and Panetta, J.: The coupled aerosol and tracer transport model to the Brazilian developments on the Regional Atmospheric Modeling System (CATT-BRAMS) – Part 1: Model description and  
15 evaluation, *Atmos. Chem. Phys.*, 9, 2843–2861, doi:10.5194/acp-9-2843-2009, 2009.
- Ganguly, D., Ginoux, P., Ramaswamy, V., Dubovik, O., Welton, J., Reid, E. A., and Holben, B. N.: Inferring the composition and concentration of aerosols by combining AERONET and MPLNET data: Comparison with other measurements and utilization to evaluate GCM output, *Geophys. Res. Lett.*, 114 (D16), D16203, 2009a.
- Ganguly, D., Ginoux, P., Ramaswamy, V., Winker, D. M., Holben, B. N., and Tripathi, S. N.: Retrieving the composition  
20 and concentration of aerosols over the Indo-Gangetic basin using CALIOP and AERONET data, *Geophys. Res. Lett.*, 36 (13), L13806, 2009b.
- Giglio, L., Descloitres, J., Justice, C. O., and Kaufman, Y. J.: An enhanced contextual fire detection algorithm for MODIS, *Remote Sens. Environ.*, 87(2 – 3), 273 – 282, doi:10.1016/S0034-4257(03)00184-6, 2003.
- Giglio, L., van der Werf, G. R., Randerson, J. T., Collatz, G. J., and Kasibhatla, P.: Global estimation of burned area using  
25 MODIS active fire observations, *Atmos. Chem. Phys.*, 6, 957 – 974, 2006.
- Ginoux, P., Chin, M., Tegen, I., Prospero, J. M., Holben, B., Dubovik, O., and Lin, S.-J.: Sources and distributions of dust aerosols simulated with the GOCART model, *J. Geophys. Res.*, 106, 20, 255 – 273, 2001.
- Ginoux, P., Horowitz, L. W., Ramaswamy, V., Geogdzhayev, I. V., Holben, B. N., Stenchikov, G., and Tie, X.: Evaluation of aerosol distribution and optical depth in the Geophysical Fluid Dynamics Laboratory coupled model CM2.1 for  
30 present climate, *J. Geophys. Res.*, 111, D22210, doi:10.1029/2005JD006707, 2006.
- Ginoux, P., Prospero, J. M., Gill, T. E., Hsu, N. C., and Zhao, M.: Global-scale attribution of anthropogenic and natural dust sources and their emission rates based on MODIS Deep Blue aerosol products, *Rev. Geophys.*, 50 (3), RG3005, 2012.



- Griffies, S. M., Winton, M., Donner, L. J., Horowitz, L. W., Downes, S. M., Farneti, R., Gnanadesikan, A., Hurlin, W. J., Lee, H. C., Liang, Z. and Palter, J. B.: The GFDL CM3 coupled climate model: characteristics of the ocean and sea ice simulations, *J. Climate*, 24(13), 3520-3544, 2011.
- Grousset, F. E., Ginoux, P., Bory, A., and Biscaye, P. E.: Case study of a Chinese dust plume reaching the French Alps. *Geophys. Res. Lett.*, 30(6), 1277, 2003.
- Haywood, J. M. and Ramaswamy, V.: Global sensitivity studies of the direct radiative forcing due to anthropogenic sulfate and black carbon aerosols, *J. Geophys. Res.*, 103, 6043-6058, 1998.
- Haywood, J. M., Ramaswamy, V., and Soden, B. J.: Tropospheric aerosol climate forcing in clear-sky satellite observations over the oceans, *Science*, 283(5406), 1299-1303, 1999.
- 10 Heald, C. L., Jacob, D. J., Park, R. J., Russell, L. M., Huebert, B. J., Seinfeld, J. H., Liao, H., and Weber, R. J.: A large organic aerosol source in the free troposphere missing from current models, *Geophys. Res. Lett.*, 32, L18809, doi:10.1029/2005GL023831, 2005.
- Hoelzemann, J. J., Longo, K. M., Fonseca, R. M., do Rosário, N. M., Elbern, H., Freitas, S. R., and Pires, C.: Regional representativity of AERONET observation sites during the biomass burning season in South America determined by correlation studies with MODIS Aerosol Optical Depth. *J. Geophys. Res.*, 114(D13), D13301, 2009.
- 15 Holben B.N., Eck, T. F., Slutsker, I., Tanré, D., Buis, J. P., Setzer, A., Vermote, E., Reagan, J. A., Kaufman, Y., Nakajima, T., Lavenu, F., Jankowiak, I., and Smirnov, A.: AERONET - A federated instrument network and data archive for aerosol characterization, *Remote Sens. Environ.*, 66, 1-16, 1998.
- Holben, B. N., Tanre, D., Smirnov, A., Eck, T. F., Slutsker, I., Abuhassan, N., Newcomb, W. W., Schafer, J. S., Chatenet, B., Lavenu, F. and Kaufman, Y. J.: An emerging ground-based aerosol climatology: Aerosol optical depth from AERONET, *J. Geophys. Res.*, 106, 12,067 –12,098, 2001.
- Horowitz, L. W., Walters, S., Mauzerall, D. L., Emmons, L. K., Rasch, P. J., Granier, C., Tie, X., Lamarque, J. F., Schultz, M. G., Tyndall, G. S. and Orlando, J. J.: A global simulation of tropospheric ozone and related tracers: Description and evaluation of MOZART, version 2, *J. Geophys. Res.*, 108 (D24), 4784, doi:10.1029/2002JD002853, 2003.
- 25 Horowitz, L. W.: Past, present, and future concentrations of tropospheric ozone and aerosols: Methodology, ozone evaluation, and sensitivity to aerosol wet removal, *J. Geophys. Res.*, 111, D22211, doi:10.1029/2005JD006937, 2006.
- Huang, Y., Wu, S., Dubey, M. K. and French, N. H. F.: Impact of aging mechanism on model simulated carbonaceous aerosols, *Atmos. Chem. Phys.*, 13, 6329-6343, 2013.
- Jaeglé, L., Quinn, P. K., Bates, T. S., Alexander, B., and Lin, J. T.: Global distribution of sea salt aerosols: new constraints from in situ and remote sensing observations, *Atmos. Chem. Phys.*, 11(7), 3137-3157, 2011.
- 30 Jaroslowski, J. and Pietruczuk, A.: On the origin of seasonal variation of aerosol optical thickness in UV range over Belsk, Poland, *Acta Geophysica*, 58 (6), 1134-1146, 2010.
- Kalnay, E., Kanamitsu, M., Kistler, R., Collins, W., Deaven, D., Gandin, L., Iredell, M., Saha, S., White, G., Woollen, J. and Zhu, Y.: The NCEP/NCAR 40-year reanalysis project, *Bull. Amer. Meteorol. Soc.*, 77(3), 437-471, 1996.



- Kiehl, J. T., Hack, J. J., Bonan, G. B., Boville, B. A., Williamson, D. L., and Rasch, P. J.: The National Center for Atmospheric Research Community Climate Model: CCM3, *J. Clim.*, 11, 1131-1149, 1998.
- Kinne, S., Schulz, M., Textor, C., Guibert, S., Balkanski, Y., Bauer, S. E., Berntsen, T., Berglen, T. F., Boucher, O., Chin, M. and Collins, W.: An AeroCom initial assessment optical properties in aerosol component modules of global models, *Atmos. Chem. Phys.*, 6, 1815-1834, 2006.
- 5 Knutson, T. R., Delworth, T. L., Dixon, K. W., Held, I., Lu, J., Ramaswamy, V., Schwarzkopf, M. D., Stenchikov, G., and Stouffer, R. J.: Assessment of Twentieth-Century regional surface temperature trends using the GFDL CM2 coupled models, *J. Clim.*, 19, doi:10.1175/JCLI3709.1, 2006.
- Koch, D., Schulz, M., Kinne, S., McNaughton, C., Spackman, J. R., Balkanski, Y., Bauer, S., Berntsen, T., Bond, T. C., Boucher, O. and Chin, M.: Evaluation of black carbon estimations in global aerosol models, *Atmos. Chem. Phys.*, 9, 9001-9026, doi:10.5194/acp-9-9001-2009, 2009.
- 10 Koffi, B., Schulz, M., Bréon, F. M., Griesfeller, J., Winker, D., Balkanski, Y., Bauer, S., Berntsen, T., Chin, M., Collins, W. D. and Dentener, F.: Application of the CALIOP layer product to evaluate the vertical distribution of aerosols estimated by global models: AeroCom phase I results, *J. Geophys. Res.*, 117, D10201, doi:10.1029/2011JD016858, 2012.
- 15 Lamarque, J. F., Bond, T. C., Eyring, V., Granier, C., Heil, A., Klimont, Z., Lee, D., Liousse, C., Mieville, A., Owen, B. and Schultz, M.G.: Historical (1850–2000) gridded anthropogenic and biomass burning emissions of reactive gases and aerosols: methodology and application, *Atmos. Chem. Phys.*, 10(15), 7017-7039, 2010.
- Lin, C. Y., Wang, Z., Chen, W. N., Chang, S. Y., Chou, C. C. K., Sugimoto, N., and Zhao, X., Long-range transport of Asian dust and air pollutants to Taiwan: observed evidence and model simulation, *Atmos. Chem. Phys.*, 7, 423–434., 2007.
- 20 Logan, T., Xi, B., Dong, X., Li, Z., and Cribb, M.: Classification and investigation of Asian aerosol absorptive properties, *Atmos. Chem. Phys.*, 13, 2253-2265, 2013.
- Lovett, R. F.: Quantitative measurement of airborne sea-salt in the North Atlantic, *Tellus*, 30(4), 358-364, 1978.
- Magi, B. I., Ginoux, P., Ming, Y., and Ramaswamy, V.: Evaluation of tropical and extratropical Southern Hemisphere African aerosol properties simulated by a climate model, *Journal of Geophysical Research*, 114 (D14), D14204, 2009.
- 25 Miller, D. J., Sun, K., Zondlo, M. A., Kanter, D., Dubovik, O., Welton, E. J., Winker, D. M., and Ginoux, P.: Assessing boreal forest fire smoke aerosol impacts on US air quality: A case study using multiple data sets, *J. Geophys. Res.*, 116(D22), D22209, 2011.
- Ming, Y., Ramaswamy, V., and Persad, G.: Two opposing effects of absorbing aerosols on global-mean precipitation, *Geophys. Res. Lett.*, 37, L13701, doi:10.1029/2010GL042895, 2010.
- 30 Naik, V., Horowitz, L. W., Fiore, A. M., Ginoux, P., Mao, J., Aghedo, A. M. and Levy II, H.: Impact of preindustrial to present-day changes in short-lived pollutant emissions on atmospheric composition and climate forcing, *J. Geophys. Res. Atmos.*, 118, 8086–8110, doi:10.1002/jgrd.50608, 2013.
- Ocko, I. B., Ramaswamy, V., Ginoux, P., Ming, Y., and Horowitz, L. W.: Sensitivity of scattering and absorbing aerosol direct radiative forcing to physical climate factors, *J. Geophys. Res.*, 117, doi:10.1029/2012JD018019, 2012.



- Ocko, I. B., Ramaswamy, Ming, Y.: Contrasting climate responses to the scattering and absorbing features of anthropogenic aerosol forcings, *J. Clim.*, 27, DOI: 10.1175/JCLI-D-13-00401.1, 2014.
- Paulot, F., Ginoux, P., Cooke, W. F., Donner, L. J., Fan, S., Lin, M. Y., ... & Horowitz, L. W.: Sensitivity of nitrate aerosols to ammonia emissions and to nitrate chemistry: implications for present and future nitrate optical depth. *Atmos. Chem. Phys.*, 16(3), 1459-1477, 2015.
- Persad, G. G., Ming, Y. and Ramaswamy, V.: The role of aerosol absorption in driving clear-sky solar dimming over East Asia. *J. Geophys. Res. Atmos.*, 119(17), 2014.
- Pietruczuk, A. and Chaikovsky, A.: Variability of aerosol properties during the 2007–2010 spring seasons over central Europe, *Acta Geophysica*, 1-21, 2012.
- Ramanathan, V. and Carmichael, G.: Global and regional climate changes due to black carbon, *Nature Geo.* 1, 221-227, doi:10.1038/ngeo156, 2008.
- Reddy, R. S. and Boucher, O.: A study of the global cycle of carbonaceous aerosols in the LMDZT general circulation model, *J. Geophys. Res.*, 109, D14202, doi:10.1029/2003JD004048, 2004.
- Reddy, M. S. and Venkataraman, C.: Inventory of aerosol and sulphur dioxide emissions from India: I—Fossil fuel combustion, *Atmos. Environ.*, 36(4), 677-697, 2002.
- Reichler, T. and Kim, J.: How well do coupled models simulate today's climate?, *Bull. Am. Meteorol. Soc.*, 89, 303, doi:10.1175/BAMS-89-3-303, 2008.
- Samset, B. H., Myhre, G., Schulz, M., Balkanski, Y., Bauer, S., Berntsen, T. K., Bian, H., Bellouin, N., Diehl, T., Easter, R. C., Ghan, S. J., Iversen, T., Kinne, S., Kirkevåg, A., Lamarque, J. F., Lin, G., Liu, X., Penner, J. E., Seland, Ø., Skeie, R. B., Stier, P., Takemura, T., Tsigaridis, K., and Zhang, K.: Black carbon vertical profiles strongly affect its radiative forcing uncertainty, *Atmos. Chem. Phys.*, 13, 2423-2434, 10.5194/acp-13-2423-2013, 2013.
- Schulz, M., Textor, C., Kinne, S., Balkanski, Y., Bauer, S., Berntsen, T., Berglen, T., Boucher, O., Dentener, F., Guibert, S. and Isaksen, I. S. A.: Radiative forcing by aerosols as derived from the AeroCom present-day and pre-industrial simulations, *Atmos. Chem. Phys.*, 6, 5225-5246, 2006.
- Shindell, D. and Faluvegi, G.: Climate response to regional radiative forcing during the twentieth century, *Nature Geo.*, 2, 294-300, doi:10.1038/NGEO473, 2009.
- Smirnov, A., Holben, B. N., Eck, T. F., Dubovik, O., and Slutsker, I.: Cloud-screening and quality control algorithms for the AERONET database, *Rem. Sens. Environ.*, 73(3), 337-349, 2000.
- Solomon, S. et al.: Technical Summary. In: *Climate Change 2007: The Physical Science Basis. Contribution of Working Group I to the Fourth Assessment Report of the Intergovernmental Panel on Climate Change* [S. Solomon, D. Qin, M. Manning, Z. Chen, M. Marquis, K. B. Averyt, M. Tignor and H. L. Miller (eds.)]. Cambridge University Press, Cambridge, United Kingdom and New York, NY, USA, 2007.
- Streets, D. G., Yarber, K. F., Woo, J.-H., and Carmichael, G. R.: Biomass burning in Asia: annual and seasonal estimates and atmospheric emissions. *Global Biogeochem. Cycles*, 17, 1099. doi:10.1029/2003GB002040, 2003.



- Tang, I. N. and Munkelwitz, H. R.: Water activities, densities, and refractive indices of aqueous sulfates and sodium nitrate droplets of atmospheric importance, *J. Geophys. Res.*, 99, 18 801–18 808, 1994.
- Tang, I. N., Tridico, A. C., and Fung, K. H.: Thermodynamic and optical properties of sea-salt aerosols, *J. Geophys. Res.*, 102, 23 269–23 276, 1997.
- 5 The World Bank: Transition to a Low-Emissions Economy in Poland, The World Bank Poverty Reduction and Economic Management Unit, Europe and Central Asia Region, February 2011, [http://siteresources.worldbank.org/ECAEXT/Resources/258598-1256842123621/6525333-1298409457335/report\\_2011.pdf](http://siteresources.worldbank.org/ECAEXT/Resources/258598-1256842123621/6525333-1298409457335/report_2011.pdf), 2011.
- Tie, X., Brasseur, G., Emmons, L., Horowitz, L., and Kinnison, D.: Effects of aerosols on tropospheric oxidants: A global model study, *J. Geophys. Res.*, 106, 2931 – 2964, 2001.
- 10 Tie, X., Madronich, S., Walters, S., Edwards, D. P., Ginoux, P., Mahowald, N., Zhang, R., Lou, C., and Brasseur, D. P.: Assessment of the global impact of aerosols on tropospheric oxidants, *J. Geophys. Res.*, 110, D03204, doi:10.1029/2004JD005359, 2005.
- Tsigaridis, K., Daskalakis, N., Kanakidou, M., Adams, P. J., Artaxo, P., Bahadur, R., Balkanski, Y., Bauer, S. E., Bellouin, N., Benedetti, A., Bergman, T., Berntsen, T. K., Beukes, J. P., Bian, H., Carslaw, K. S., Chin, M., Curci, G., Diehl, T., Easter, R. C., Ghan, S. J., Gong, S. L., Hodzic, A., Hoyle, C. R., Iversen, T., Jathar, S., Jimenez, J. L., Kaiser, J. W., Kirkevåg, A., Koch, D., Kokkola, H., Lee, Y. H., Lin, G., Liu, X., Luo, G., Ma, X., Mann, G. W., Mihalopoulos, N., Morcrette, J. J., Müller, J. F., Myhre, G., Myriokefalitakis, S., Ng, N. L., O'Donnell, D., Penner, J. E., Pozzoli, L., Pringle, K. J., Russell, L. M., Schulz, M., Sciare, J., Seland, Ø., Shindell, D. T., Sillman, S., Skeie, R. B., Spracklen, D., Stavrakou, T., Steenrod, S. D., Takemura, T., Tiitta, P., Tilmes, S., Tost, H., van Noije, T., van Zyl, P. G., von Salzen, K., Yu, F., Wang, Z., Wang, Z., Zaveri, R. A., Zhang, H., Zhang, K., Zhang, Q., and Zhang, X.: The AeroCom evaluation and intercomparison of organic aerosol in global models, *Atmos. Chem. Phys.*, 14, 10845-10895, 10.5194/acp-14-10845-2014, 2014.
- 15
- VanCuren, R. and Cahill, T.: Asian aerosols in North America: Frequency and concentration of fine dust, *J. Geophys. Res.*, 25 107, 4804, doi:10.1029/2002JD002204, 2002.
- Venkataraman, C., Habib, G., Kadamba, D., Shrivastava, M., Leon, J.-F., Crouzille, B., Boucher, O., and Streets, D. G.: Emissions from open biomass burning in India: Integrating the inventory approach with high-resolution Moderate Resolution Imaging Spectroradiometer (MODIS) active-fire and land cover data, *Global Biogeochem. Cycles*, 20, GB2013, doi:10.1029/2005GB002547, 2006.
- 30 Westphal, D. L. and Toon, O. B.: Simulations of microphysical, radiative, and dynamical processes in a continental-scale forest fire smoke plume, *J. Geophys. Res.*, 96, 22,379 – 22,400, 1991.
- Winker, D. M., Hunt, W. H., and McGill, M. J.: Initial performance assessment of CALIOP, *Geophys. Res. Lett.*, 34, L19803, doi:10.1029/2007GL030135, 2007.



Winker, D. M., Tackett, J. L., Getzewich, B. J., Liu, Z., Vaughan, M. A., and Rogers, R. R.: The global 3-D distribution of tropospheric aerosols as characterized by CALIOP, *Atmos. Chem. Phys.*, 13, 3345–3361, doi:10.5194/acp-13-3345-2013, 2013.

5 Wong, M. S., Nichol, J. E., and Lee, K. H.: Estimation of aerosol sources and aerosol transport pathways using AERONET clustering and backward trajectories: a case study of Hong Kong. *Inter. J. Rem. Sens.*, 34 (3), 938-955, 2013.



		CM2.1	CM3
<b>Total Aerosol</b>	Aerosol Optical Depth	0.17	0.16
	Absorption Optical Depth	0.01	0.008
	Scattering Optical Depth	0.16	0.15
<b>Black Carbon</b>	Emissions (TgBC yr <sup>-1</sup> )	11	8.2
	Burden (µg m <sup>-2</sup> )	550	270
	Aerosol Optical Depth	0.008	0.004
	Absorption Optical Depth	0.006	0.0009
	Scattering Optical Depth	0.002	0.003
<b>Sulfate</b>	Emissions (TgSO <sub>2</sub> yr <sup>-1</sup> )	147	108
	Burden (µg m <sup>-2</sup> )	5000	3500
	Aerosol Optical Depth	0.1	0.07
	Absorption Optical Depth	0	0.004
	Scattering Optical Depth	0.1	0.06
<b>Organic Carbon</b>	Emissions (TgC yr <sup>-1</sup> )	52	75
	Burden (µg m <sup>-2</sup> )	2700	3600
	Aerosol Optical Depth	0.01	0.03
	Absorption Optical Depth	0	0.008
	Scattering Optical Depth	0.01	0.03
<b>Dust</b>	Emissions (Tg yr <sup>-1</sup> )	1960	1221
	Burden (µg m <sup>-2</sup> )	44000	27000
	Aerosol Optical Depth	0.03	0.018
	Absorption Optical Depth	0.005	0.002
	Scattering Optical Depth	0.02	0.016
<b>Sea Salt</b>	Emissions (Tg yr <sup>-1</sup> )	NA <sup>a</sup>	6188
	Burden (µg m <sup>-2</sup> )	9800	12800
	Aerosol Optical Depth	0.02	0.04
	Absorption Optical Depth	0	0
	Scattering Optical Depth	0.02	0.04

**Table 1: Global-mean present-day aerosol properties as simulated by CM2.1 (1996-2000) and CM3 (2000-2004). Emissions data for year 2000. (a) See text for details.**

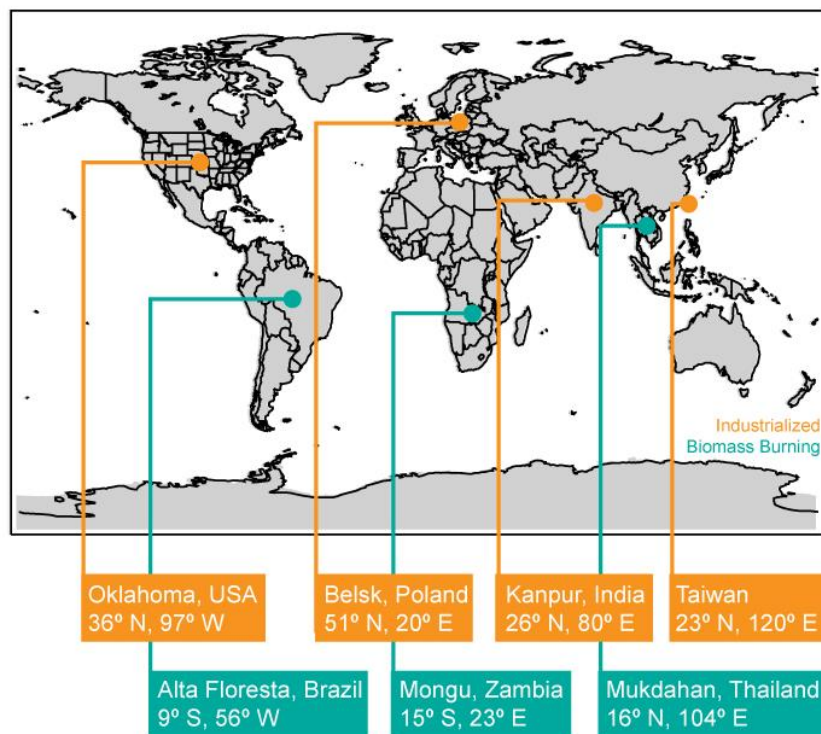
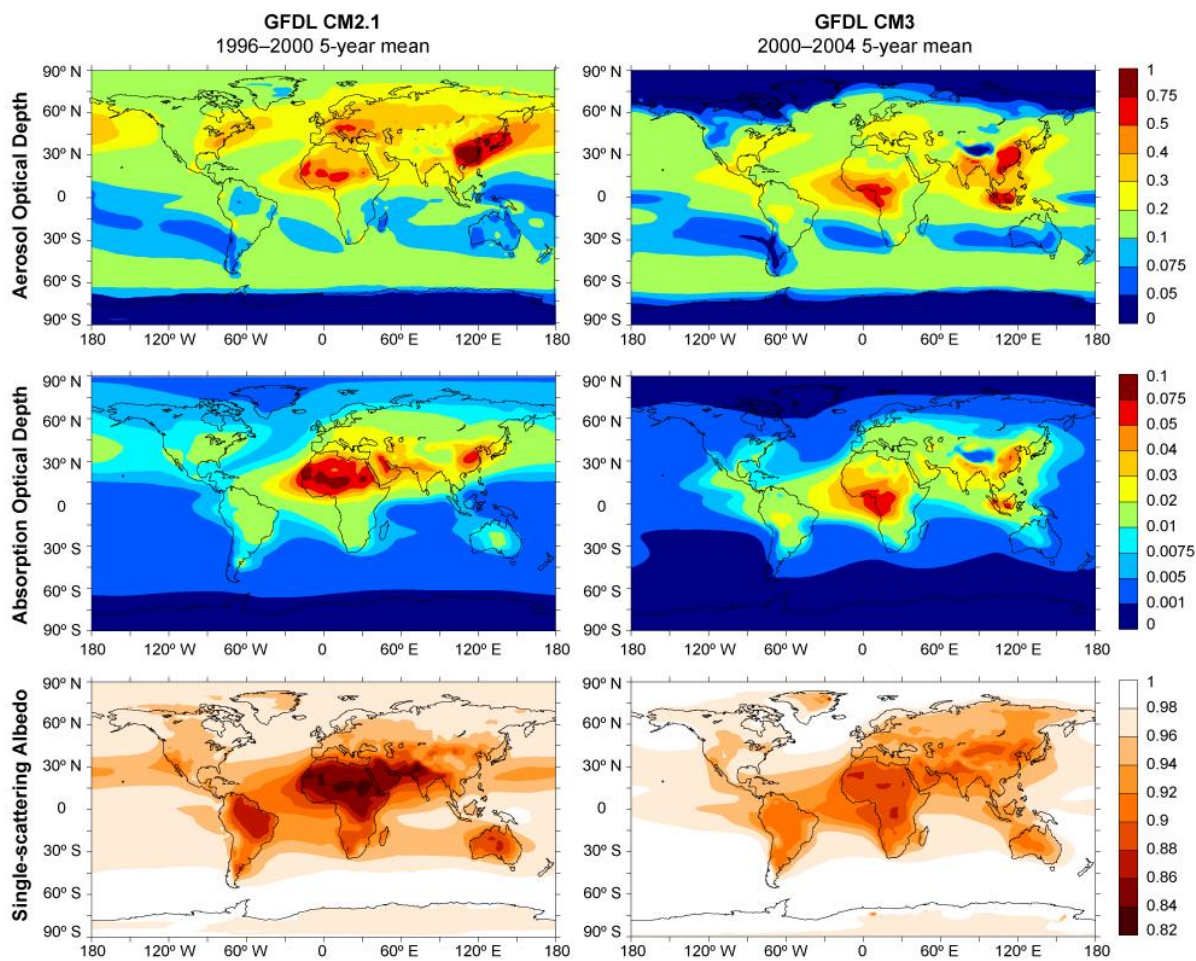
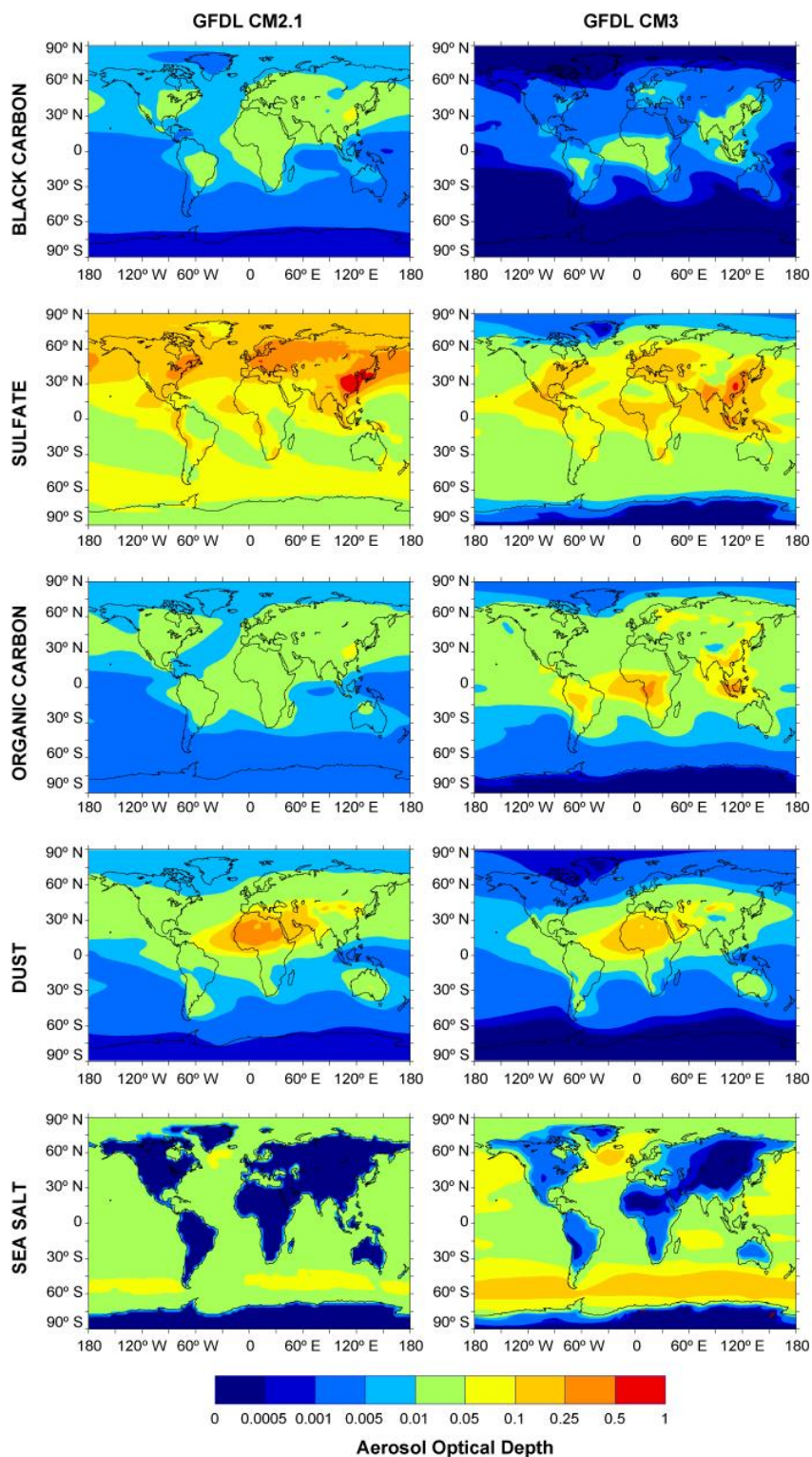


Figure 1: Map of locations of comparison sites.



**Figure 2: Model-derived total aerosol optical properties. Five-year annual means from a 5-member historical simulation ensemble, CM2.1 present-day from 1996–2000, CM3 present-day from 2000–2004.**





**Figure 3: Model-derived aerosol optical depth by component. Five-year annual means from a 5-member historical simulation ensemble, CM2.1 present-day from 1996–2000, CM3 present-day from 2000–2004.**

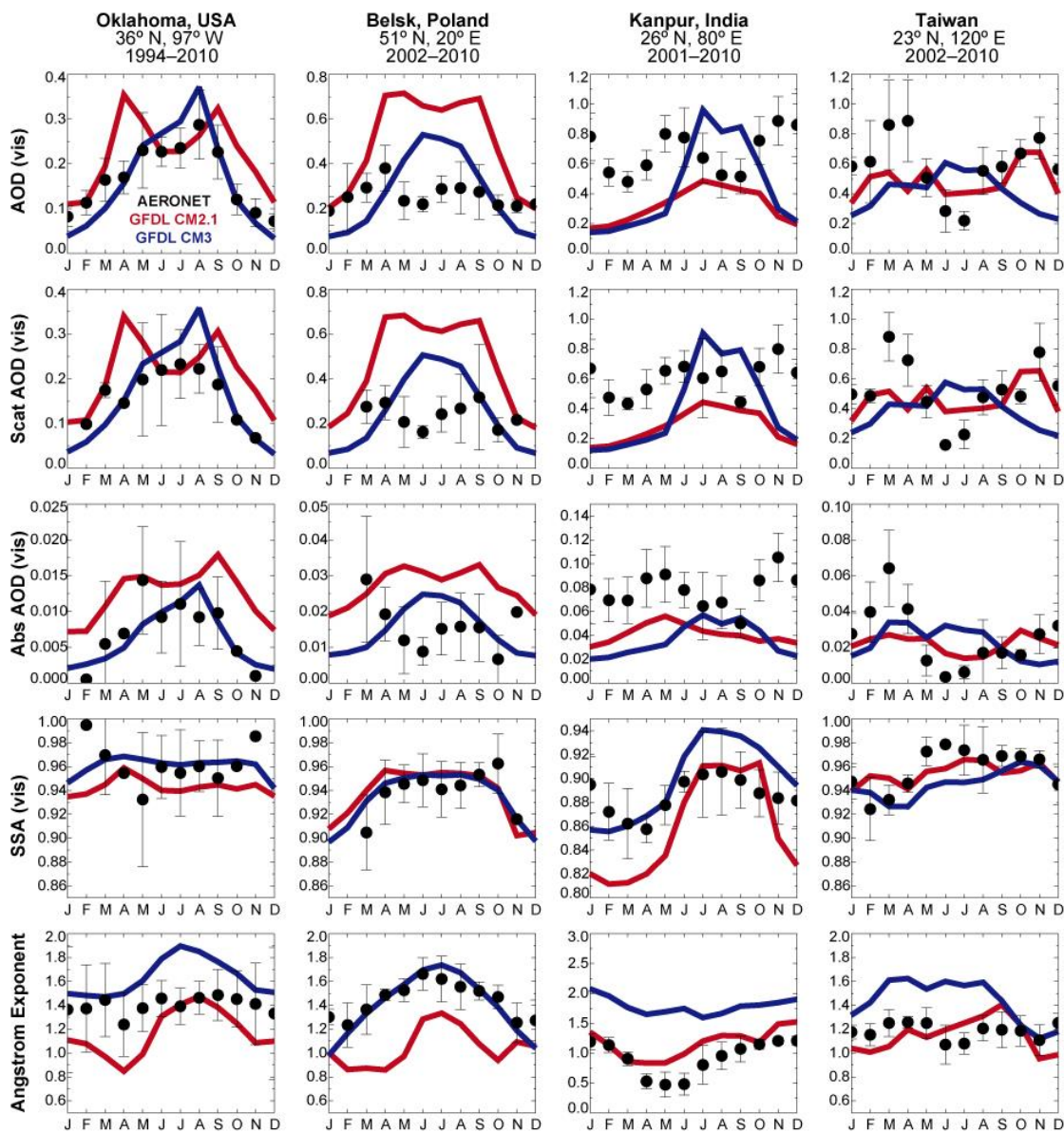


**Figure 4: Optical properties from AERONET and the models for industrialized region sites. AERONET optical properties measured at 440 nm, model optical properties derived for 550 nm.**

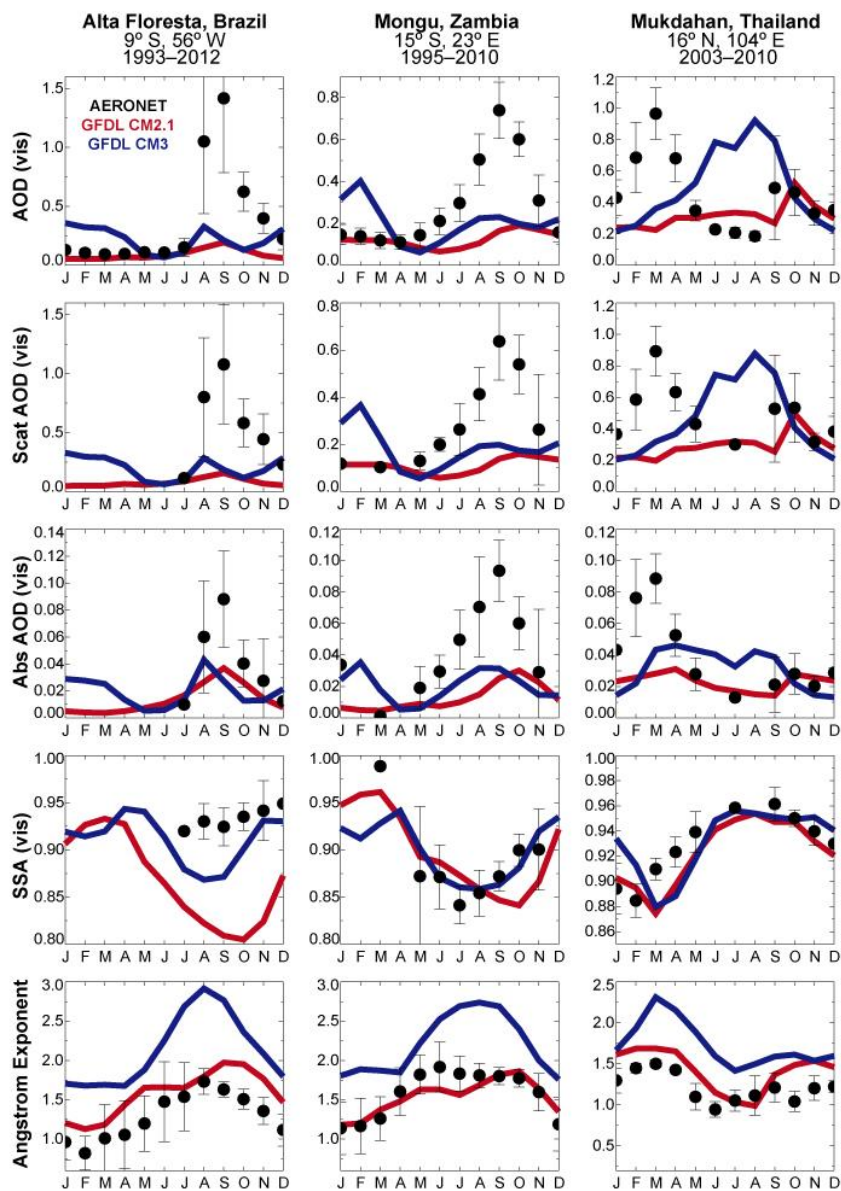


Figure 5: Optical properties from AERONET and the models for biomass burning region sites. AERONET optical properties measured at 440 nm, model optical properties derived for 550 nm.

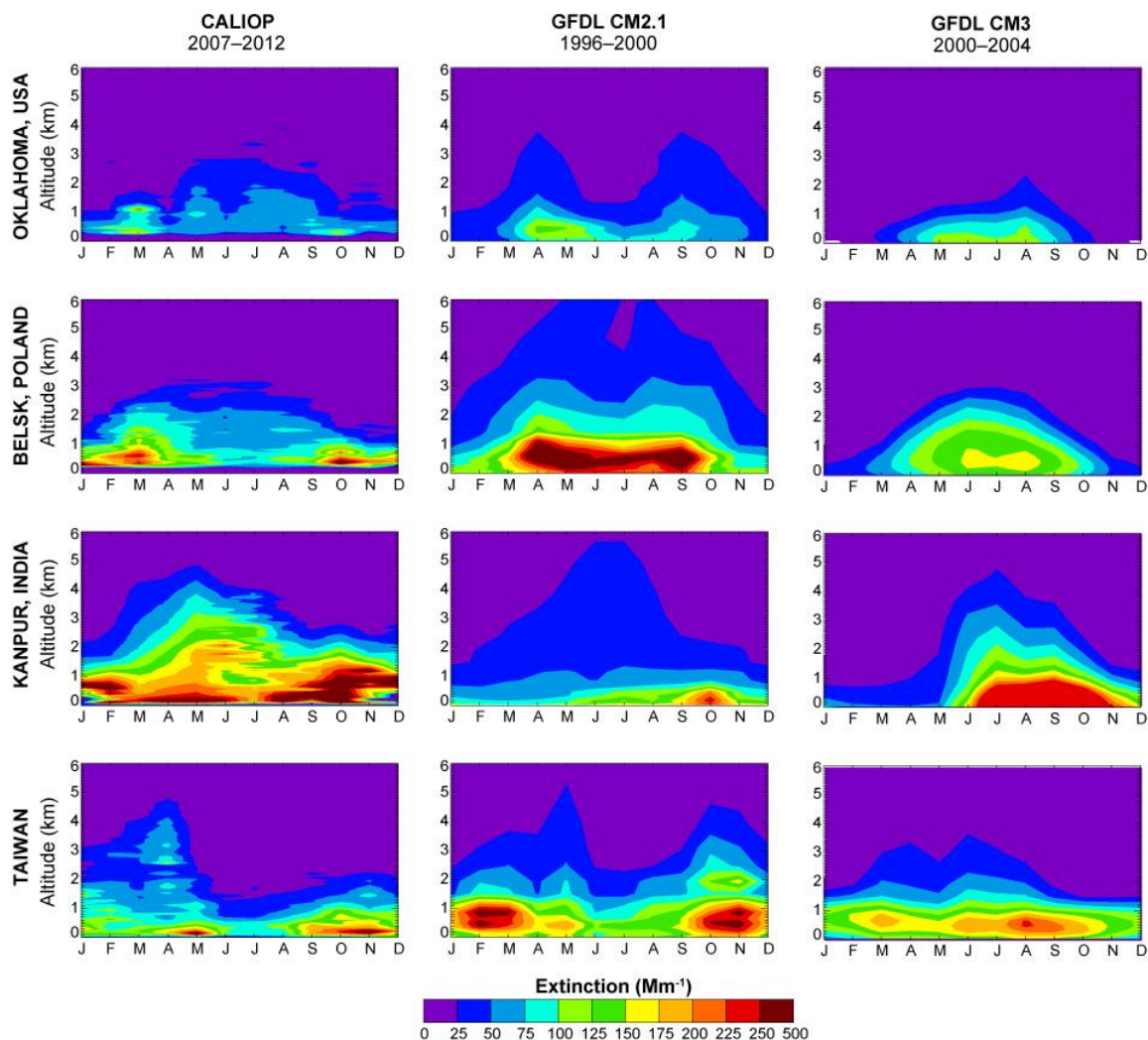


Figure 6: Extinction coefficients from CALIOP and the models for industrialized sites. CALIOP extinctions measured at 550 nm, model parameters derived for 550 nm.

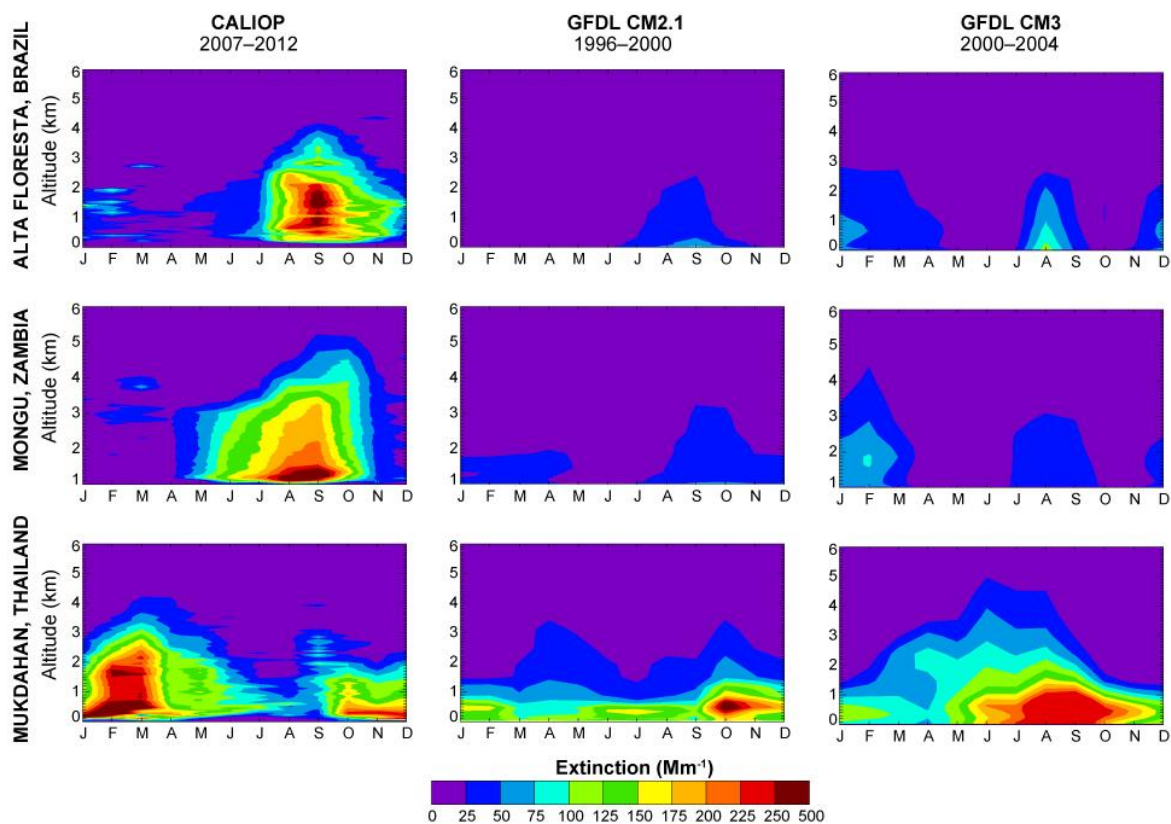


Figure 7: Extinction coefficients from CALIOP and the models for biomass burning sites. CALIOP extinctions measured at 550 nm, model parameters derived for 550 nm.